Fermi National Accelerator Laboratory

FERMILAB-Pub-96/328-A
September 1996

Weak Lensing On the Celestial Sphere

ALBERT STEBBINS

NASA/Fermilab Astrophysics Center, FNAL, Box 500, Batavia, Illinois 60510, USA

ABSTRACT. This paper details a description of the pattern of galaxy image distortion over the entire sky caused by the gravitational lensing which is the result of large scale inhomogeneities in our universe. We present a tensor spherical harmonic formalism to describe this pattern, giving many useful formulae. This is applied to density inhomogeneities, where we compute the angular power spectrum of the shear pattern, as well as the noise properties due to finite galaxy sampling and cosmic variance. We show that a detectable level of shear is present for very nearby galaxies, $z \lesssim 0.2$. For such a shallow sample much of the largest signal-to-noise comes from very large angular scales, $\theta \gtrsim 10^\circ$, although it is in the form of very small shear at a level $\lesssim 10^{-3}$.

1. Introduction

In recent years gravitational lenses have provided a set of extremely useful tools for understanding the universe around us. One of these tools, sometimes called the orientation correlation function or OCF, is a method whereby one searches for alignments in the orientations of galaxies on the sky (Tyson, Valdes, and Wenk 1990). Such alignments will be caused by the deflection of light by the gravitational field of mass concentrations in front of the galaxies one is observing. In the weak lensing approximation the OCF is determined by the *shear* of the image deformation caused by this bending of light. Large format CCD's have made such observations of weak lensing shear possible and there have been numerous studies of the mass concentration in clusters of galaxies with this technique (Tyson, Valdes, and Wenk 1990, Bonnett, Meiler & Fort 1994, Fahlman *et al.* 1994, Smail, Ellis & Fitchett 1994, Smail & Dickinson 1995, Tyson and Fisher 1995, Squires *et al.* 1996a&b, Luppino & Kaiser 1996). It is in the direction of clusters of galaxies at moderate redshift where the shear is liable to be greatest and the size of the central parts of such clusters is a good fit with the typical field of view of many CCD cameras, i.e. about $5'$. Away from the direction of clusters of galaxies the shear is liable to be much smaller. In principle one should be able to detect very small shears by looking for alignments among a greater number of background galaxies. One might obtain these greater numbers either by taking deeper images, which has the advantage that shear will increase with depth, or by looking at larger areas on the sky. With the advent of very large CCD mosaic cameras with a large field of view one can expect much wider area surveys looking for weak lensing shear. A limiting factor in such wide surveys is the small amplitude of the shear one is trying to measure, and further study is required to see just how small one can reduce systematic errors when looking for galaxy alignments.

One of the most interesting applications of weak lensing which is to map the mass distribution as close to the local neighborhood as possible. This will allow a comparison of the galaxy distribution and the mass distribution which should help us to understand galaxy formation and biasing. Gould and Villumsen (1994) have pointed out that the Sloan Digital Sky Survey (see Kent 1994 for a description of the "SDSS") which is imaging one quarter of the sky should be able to measure the mass distribution around the Coma cluster. Whether this goal is achievable depends on the level of non-correctable systematic errors, however even if present imaging surveys are not successful one can expect that very large area weak lensing surveys will be achieved sometime in the future.

Predictions of the angular distribution of shear and amplification on the sky has been made in the context of the small areas on the sky where the small angle approximation is utilized (Blandford *et al.* 1991, Miralda-Escudé 1991, Kaiser 1992, Kaiser and Squires 1993). This is quite natural given that most weak lensing observations would be limited to extremely small patches on the sky. However looking ahead to a time when the area on the sky surveyed becomes large, such as in the SDSS, one will need to go beyond the small angle approximation in order to characterize the weak lensing pattern one observes. This is not to say that the lensing deflection angles will be large, they will not, but rather that when the area on the sky becomes large one needs to take into account the "curvature" of the celestial sphere when computing things like shear-shear correlation functions. Since the shear is not a scalar quantity, but rather a rank-2 tensor, one can not simply use the the scalar spherical harmonic expansion. In this paper is presented a tensor spherical harmonic expansion which the author feels is rather well suited to describing the shear pattern. Most published expositions of tensor spherical harmonics were motivated by describing 3-d tensor gravitational fields

and these expositions are complicated by the additional formalism needed to describe the 3rd dimension (see Thorne (1980) for a review). The formalism described here is rather simpler as it is restricted to symmetric traceless tensor fields on the 2-d sphere. Although developed independently this formalism is very close to that of Zerilli (1970).

The paper is arranged as follows. In §2 we describe the decomposition of the shear pattern into two geometrically distinct types in a formalism which is easily generalizable from the small-angle approximation to the celestial sphere. In §3 is considered the various approximation used when computing the image distortion in lensing. In §4 is presented the tensor spherical harmonic decomposition of the shear, with a large number of useful identities. In §5 the tensor harmonic expansion is used to work out the formalism to describe the shear pattern produced by density perturbations in an Einstein-deSitter universe. In §7 we estimate the accuracy one might expect to obtain in measurements of the shear due to the "shot noise" from the finite number of galaxies that are available to probe the shear, and to "cosmic variance" (finite sampling). In §7 the formalism developed is applied to a phenomenological model of the density perturbations in our universe and illustrate the type of shear pattern one might expect to find and how it compares to the shot noise and cosmic variance. In §8 we summarize the results.

2. Scalar and Pseudo-Scalar Shear

The shear gives the degree to which images of objects we see on the sky are elongated, after factoring out the intrinsic shape of the actual objects. The shear at a point has an amplitude and a direction and may be described by a symmetric traceless matrix, i.e.

$$\gamma_{ab} = \gamma \begin{pmatrix} \cos 2\varphi & \sin 2\varphi \\ \sin 2\varphi & -\cos 2\varphi \end{pmatrix}. \tag{2.1}$$

Here γ measures the amplitude and φ the direction wrt to some fiducial position angle on the sky. Of course the direction is modulo π not 2π since stretching an image in one direction is the same as stretching it in the opposite direction. Note that rotating the direction of the shear by 90° changes the sign of the the shear, while rotating the shear by ±45° produces a shear which is orthogonal to the original, in the sense that $\gamma^{ab}\gamma'_{ab} = 0$. (The Einstein summation convention is used here and throughout this paper.) Whether one rotates 45° to the right or 45° to the left changes the sign of the shear. One can construct any shear matrix by linear combinations of a given shear matrix and one rotated by 45°.

Here we are concerned with shear fields on the sky. In this section we consider the small angle approximation where the sky is approximated as a Euclidean plane. One may write any shear field on a plane as a Fourier decomposition, e.g.

$$\gamma_{ab}(\vec{x}) = -\frac{1}{2\pi}\int d^2\vec{q}\left[\phi^{\oplus}(\vec{q})\left(f_{,ab} - \frac{1}{2}\nabla^2\delta_{ab}f\right) + \phi^{\otimes}(\vec{q})\,\frac{1}{2}\left(f_{,ac}\epsilon^c{}_b + f_{,cb}\epsilon^c{}_a\right)\right] \qquad f(\vec{q},\vec{x}) = e^{i\vec{q}\cdot\vec{x}} \tag{2.2}$$

where $\vec{q}$ is the 2-d wavenumber on the (planar) sky and

$$f_{,ab} = \frac{\partial^2}{\partial x^a \partial x^b} \qquad \epsilon^a{}_b = \begin{pmatrix} 0 & 1 \\ -1 & 0 \end{pmatrix}. \tag{2.3}$$

The tensor $\epsilon^a{}_b$ is known as the Levi-Civita symbol in 2-d. The $\gamma^{\oplus}$ modes have shear directed parallel to $\vec{q}$ while the $\gamma^{\otimes}$ modes have shear rotated 45° to the right from the $\vec{q}$ direction. This is all one needs to construct an arbitrary shear field.

Since the $\gamma^{\oplus}$ modes are just given by derivatives of the scalar mode function $f(\vec{q},\vec{x})$ we will refer to this part of the shear as the ***scalar shear***. The $\gamma^{\otimes}$ modes are a geometrically distinct component of the shear, given by the 2nd derivative matrix of f but multiplied by the $\epsilon^c{}_b$ which has the effect of rotating the scalar shear by 45° to the right in a right-handed coordinate system or 45° to the left in a left-handed coordinate system. A change in the handedness would have the effect of multiplying the pseudo-scalar shear tensor by -1. This sign difference depending on the handedness of the coordinate system means that the component of the shear transforms as a pseudo-scalar rather than a scalar, and it is called the ***pseudo-scalar*** component of the shear. The two types of shear pattern are illustrated in fig 1. One can represent any pattern of shear by a sum of scalar and pseudo-scalar shear

The decomposition we have just described is similar to the decomposition of a vector field into it's vortical and non-vortical parts. Note however that in 3-d for each Fourier mode their are two linearly independent vortical

components and one must choose a azimuthal angle about the wavenumber to specify one. For this reason one cannot write these vortical modes in terms of derivatives of the scalar modes $e^{i\mathbf{k}\cdot\mathbf{x}}$ plus a handedness as this will not specify *the* azimuthal angle. In 2-d one may express arbitrary vector and tensor fields in terms of scalar functions Levi-Civita symbols, as we have done above. There is not the distinction between scalar, vector, and tensor components of fields higher dimensions.

In the usual treatment of gravitational (or non-gravitational) lensing, one thinks of the lensing as being a displacement field on the sky, i.e. in a given direction on the sky what one sees is at a true position in space which is the apparent position displaced by some amount, $\vec{\Delta}$. This is what we will later call the ***displacement approximation***. For arbitrary gravitational perturbations it is problematic to define what the apparent position is a hence what the displacement field is. In the next section it is argued that for weak fields it is an excellent approximation to treat the lensing as a displacement field on an unperturbed space-time and this is the approximation we will use here. Let us denote the displacement from apparent to true position on the planar sky by $\vec{\Delta}$. The 2×2 deformation matrix is given by

$$\psi_{ab} = \delta_{ab} + \Delta_{a,b} = (1-\kappa)\,\delta_{ab} - \gamma_{ab} + \omega\,\epsilon_{ab} \tag{2.4}$$

which we have decomposed into term which gives the trace, a term which gives the symmetric traceless part, and a term which gives the anti-symmetric part. The trace gives the ***expansion***, κ, the traceless symmetric part give the shear, γ_{ab}, and the anti-symmetric part gives the ***rotation***, ω. The image amplification is $1/((1-\kappa)^2 - \gamma^2 + \omega^2)$ or approximately $1 + 2\kappa$ in the weak lensing limit. An arbitrary displacement field can also be written as a Fourier integral of scalar and pseudo-scalar components:

$$\Delta_a(\vec{x}) = -\frac{1}{2\pi}\int d^2\vec{q}\,\left[\phi^{\oplus}(\vec{q})\,f_{,a} + \phi^{\otimes}(\vec{q})\,f_{,c}\epsilon^{c}{}_{a}\right] \qquad f(\vec{q},\vec{x}) = e^{i\vec{q}\cdot\vec{x}}. \tag{2.5}$$

Note that $f_{,c}\epsilon^{c}{}_{a}$ rotates the gradient of f by $90°$. When the deformation is given by a displacement field on a Euclidean plane we find the following relations

$$\nabla^2\kappa = +\gamma^{ab}{}_{,ab} \qquad \nabla^2\omega = -\gamma^{ab}{}_{,ac}\epsilon^{c}{}_{b}. \tag{2.6}$$

Since ∇^2 is invertible the scalar shear is given by the expansion, κ, while the pseudo-scalar shear by the rotation, ω. A scalar and pseudo-scalar displacement field is illustrated in figure 1.

It is unlikely that anything other than density inhomogeneities contribute significantly to the shear in our universe. These density inhomogeneities produce scalar metric perturbations. One shouldn't confuse the "scalar"-ness of density perturbations which has to do with transformation properties in 3 spatial dimensions, with the "scalar"-ness of the shear which has to do with transformation properties on the 2-dimensional sky. Nevertheless it is true that 3-d scalar perturbations will only produce 2-d scalar shear, at least in the weak lensing limit. In contrast tensor and vector metric perturbations will contribute to both scalar and pseudo-scalar shear, however we expect this to be very small. Thus we really do not expect there to be any significant pseudo-scalar shear. We have chosen to include pseudo-scalar shear in our analysis for a variety of reasons. Most importantly because the pseudo-scalar shear is part of what one measures when one looks at galaxy alignments, and one should not leave it out of ones analysis. Also, one never knows, maybe the pseudo-scalar shear field is not negligible, one should measure it and see!

Kaiser (1992) noted that the redundant information in the shear field could provide a useful check of ones observation. One can determine the pseudo-scalar ω in the same way one determines the scalar κ if one first rotates the galaxy position angles by $45°$, and then one should check that the derived ω is is consistent with zero. (Kaiser *et al.* 1994; A. Tyson private communications; Stebbins, McKay, and Frieman 1996). Just such a procedure has been implemented in Luppino and Kaiser (1996) where they compare $\gamma^{ab}{}_{,ab}$ to $\gamma^{ab}{}_{,ac}\epsilon^{c}{}_{b}$ showing that the latter is indeed much smaller than the former in the field of the cluster of galaxies ms1054-03, and consistent with zero.

3. Approximations

In this paper we make predictions of extremely small image deformation. These are calculated using a number of approximations and one must be careful that the approximations are accurate enough so that these predictions are accurate. In other words one must be sure that there are not other small but significant contribution to the lensing which are not included. Many approximations become more accurate as the image deformation becomes smaller, while others do not. In this section we identify most of the approximations used here. None of these approximations are new

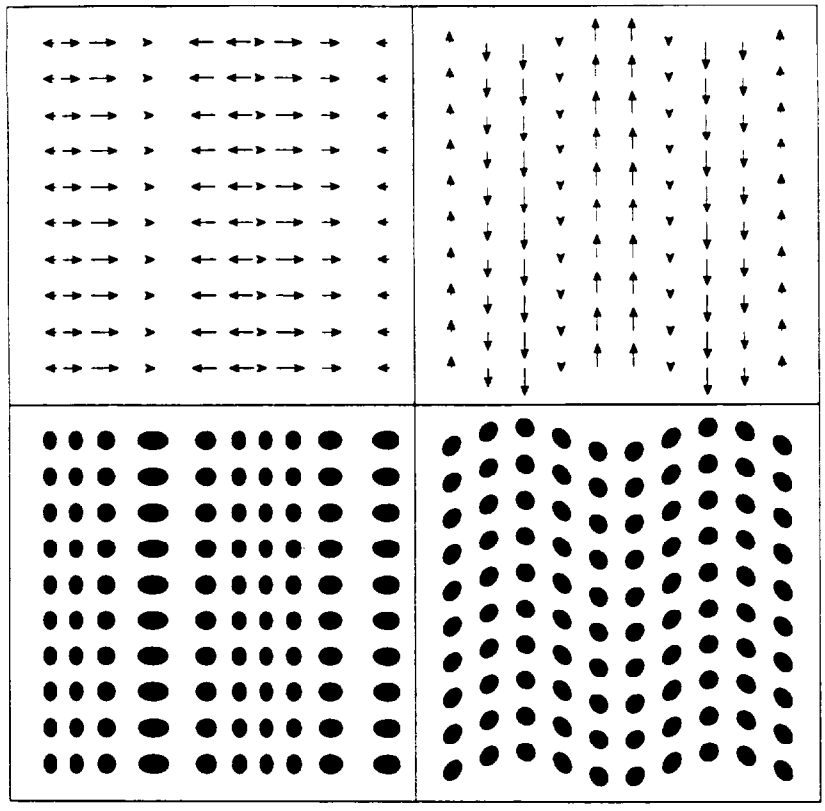

Figure 1: In the top left panel is shown a *scalar* pattern of gravitational deflections. Scalar deflections are parallel (or anti-parallel) to the direction of variation of the deflection. In the top right panel is shown a *pseudo-scalar* pattern of gravitational deflections. Pseudo-scalar deflections are $\pm 90°$ from the direction of variation of the deflection. For an arbitrary pattern of gravitational deflections one will transform the scalar components of the deflections into pseudo-scalar components and vice versa by rotating the deflection direction by 90°. Plotted in the bottom left panel is a scalar pattern of ellipticities generated by applying the deflections in the top left panel to a square array of circles. Scalar shear produces ellipticity patterns which are parallel and perpendicular to the (horisontal) direction of variation of the ellipticities. Scalar shear produces images which are magnified or demagnified. In the bottom right panel is shown the pattern of ellipticities induced by a the deflections in the top left panel. Pseudo-scalar ellipticities oscillate between being $+45°$ and $-45°$ from the direction of variation. In the weak lensing limit pseudo-scalar shear does not amplify the images. One will transform the scalar components of the shear pattern into pseudo-scalar components of shear and vice versa by rotating the object ellipticities by 45°. Such a transformation will not change the magnification or the displacement of the objects on the sky, so rotated scalar shear will still exhibit (de)magnification while rotated pseudo-scalar shear will not. While shear patterns cannot always be treated as the result of a deflection it is usually a good approximation to do so.

to this work, and not all studies of gravitational lensing make use of all of the approximations used here. Below we will use the geometric optics approximation in weak field gravity for perturbations from Friedman-Robertson-Walker space-times. These are clearly excellent approximations for cosmology. It is generally assumed that we are in the "weak lensing" limit, namely that the deformation tensor of eqs (2.4) & (4.1) are close to the identity matrix, although many of the formulae are true even for strong lensing. For isolated regions around galaxy clusters, galaxies, and stars weak lensing will not be a valid approximation, and generally as one goes to smaller angular scales the stronger the lensing becomes. To what extent effects from small scale strong lensing creep into larger scales is a subject which needs further study.

When computing image distortion we integrate the perturbation to a beam of photons along the unperturbed path of the photons. To do otherwise would be to include terms which are formally 2nd order in the metric perturbation so one can argue that this is part of the weak lensing approximation. Even when the image distortion is large this may also be a good approximation if the statistical properties of matter field which one traverses on the perturbed trajectory are quite similar to that traversed on the unperturbed trajectory. However the argument that density perturbations only produce scalar patterns of shear rests largely on the assumption that it is valid to use the unperturbed trajectory. In general for strong lensing one can expect density perturbations to produce both scalar and pseudo-scalar shear. An exception occurs when the mass which produce the strong lensing is localized to a narrow range of distances. In

this case one can still use the unperturbed trajectory to compute the total deflection accurately. Thus in studies of lensing around individual galaxies or galaxy clusters one can assume that the shear pattern is purely scalar since it is unlikely that two large mass concentrations will line-up sufficiently to contributed significantly to the lensing. However on small enough angular scales the strong lensing will be due to a variety of objects along the line-of-sight and the shear pattern will contain both scalar and pseudo-scalar components. Again further study should be done on the contamination by small scale strong lensing of larger scale weak lensing.

One approximation which is important for this paper is what will be called the ***deflection approximation***. Namely that one can think of the effect of gravitational lensing as a deflection, where the light has been deflected from a "straight path" in an underlying flat geometry. While this is a perfectly valid description for lenses made of refractive materials in flat space, it is only an approximation for gravitational lensing. This is because there really is no underlying flat geometry, after all the light is deflected because the space is not flat. Below we will argue that in the cases of interest the space is flat enough so that this deflection approximation is a good one. Even though in this paper we consider very weak lensing, the image distortions we consider are still much weaker than the intrinsic distortion pattern caused by the curvature of spacetime. Note that this is not an intrinsic property of the weak lensing approximation, but rather has more to do with how the amplitude of metric perturbations in our universe vary with scale. If we had very large perturbations entering the horizon today much of the image distortion would be a result of the global geometry rather than the deflection.

Let us try to make these ideas more precise. In §5 of this paper we consider the lensing due to density perturbations. The deflection as a function of distance from the observer is computed using the metric evaluated on the unperturbed path, i.e. by twice integrating the "gravitational acceleration" of the photon perpendicular to the unperturbed path. With this deflection we compute the intersection of both the unperturbed trajectory and the "deflected trajectory" with a surface defined by a fixed coordinate distance from the observer, i.e. $r = \sqrt{x^2 + y^2 + z^2}$, which we will call the "source sphere". We use the the Jacobian of the mapping of the Newtonian coordinates from the deflected position on the source sphere to the undeflected position as the deformation tensor in eqs (2.4) or (4.1). This procedure has some obvious failings. Firstly if the photons do not intersect the source sphere at right angles then even for photons which are not focused or sheared the Jacobian matrix will contain an eigenvalue of $1/\cos\theta$ where θ is angle between the normal to the surface and the direction of the perturbed photon trajectory. Thus even if there is no true image distortion one would infer a de-amplification and shear. This error is not large, in the sense that the leading error is $\propto \theta^2$, so is an insignificant error in the sense of weak lensing. In cosmology the deflections are rarely greater than 10^{-4} radians even when the lensing is strong. A more worrisome error comes from the fact that the source sphere defined above is not truly spherical in geometry. Scalar perturbations in Newtonian gauge have an isotropic metric so the intrinsic geometry of the source sphere does not lead to any spurious shear. However a small coordinate patch spanning a coordinate area A on the source will actually spans a physical area $(1 - 2\Phi/c^2)A$ where Φ is the Newtonian gravitational potential. Unless one corrects for this one will add a spurious contribution to the expansion, κ, of $2\Phi/c^2$. Since this contribution to κ is linear in the metric perturbation it does not become arbitrarily smaller than the true signal in the weak lensing limit. However, for our own universe we know that $\Phi \lesssim 10^{-5}c^2$ while, as we will see below, $\kappa \gtrsim 10^{-4}$. Thus by ignoring the intrinsic geometry of the source sphere we only make a small error. As mentioned above, the reason for this fortuitous numerology has to do with the shape of the power spectrum. No such fortuitous numerology applies to the case of gravitational lensing from gravitational radiation, so one cannot use the deflection approximation in this case. We do not consider lensing from gravitational radiation in this paper. We will ignore the intrinsic geometry of the source sphere in the rest of the paper. While it is not terribly cumbersome to include this term, it would invalidate the simple and accurate relationship between the different components of the image distortion, κ, ω, and γ_{ab} as expressed in eq (2.6), or implicitly in eq (4.10).

A more general treatment of image distortion, can be gotten from the optical scalar equation (e.g. Hawking & Ellis 1973; Schneider, Ehlers, & Falco 1992) whereby one measure the distortion of a bundle of light rays with respect to an orthonormal basis parallel transported along with the light rays from the observer. This approach makes no approximation other than assuming the validity of geometric optics. It would be too cumbersome for our purposes to use this approach on unperturbed trajectories, i.e. to use ray-tracing. One could approximate the optical scalar equation by implementing the same procedure along an unperturbed trajectory. One property of the optical scalar equation which is something of a drawback is that since the parallel transported basis vectors will rotate with the photons, this method does not yield any information on image rotation. While in the case of strong gravitational fields it is difficult to make a sensible definition of image rotation, in the case of weak fields where the image distortion is generally much larger than the metric perturbation there is a real sense in which images may be rotated and it would be useful to include this effect in ones computations.

In §5 and afterwards a set of assumptions and simplifications are implemented. We do only consider a flat matter-dominated Einstein-deSitter cosmology, although one could clearly generalize all of formulae to open or closed cosmologies with or without a cosmological constant. The formulae used in §5&§7 assume that the perturbations grow according to linear theory. This is a good approximation on large scales $\gtrsim 10\,h^{-1}$Mpc but we when we consider the shear at shallow depths we do venture into a regime where linear theory is not appropriate. In fact the model power spectrum in §7 is no-linear on scales of interest. One could try to correct this by having the power spectrum vary as one looks back in time, i.e. with radius. Since the results presented here are meant to be illustrative this approach is not warranted. In any case since the emphasis is of this paper is on shallow surveys these sorts of corrections are liable to be small.

4. Decomposition of Shear on the Celestial Sphere

Even though the coherence in the shear field falls off with separation there will be some small coherence even over very large angles on the sky. To understand this large angle coherence one must take into account that the sky is a sphere and not a plane. Here we consider the weak lensing on the celestial sphere, i.e. the sphere of the sky. For the moment we consider the image deformation at a fixed distance but later generalize the analysis to include the fact that the galaxies whose images are distorted span a range of distances. Thus we have the a mapping from the direction in which you are looking, $\hat{\mathbf{n}}$, to the direction you are looking at, $\hat{\mathbf{m}}$, at a given distance, r. The effect of the lensing is to displace the photon trajectory at a given distance by the 3-d vector $\Delta = \hat{\mathbf{m}} - \hat{\mathbf{n}}$. If the angle by which the light rays are bent are sufficiently small then Δ and $\hat{\mathbf{n}}$ are nearly perpendicular so that we may approximate Δ as being in the tangent space of the the direction sphere $\hat{\mathbf{n}}$, i.e. $\Delta(r)$ is a vector field on the sphere. As in §2 we may define the deformation tensor and it's various components

$$g_{a\flat} + \Delta_{a:\flat} = \psi_{a\flat} = (1-\kappa)\,g_{a\flat} - \gamma_{a\flat} + \omega\epsilon_{a\flat} \tag{4.1}$$

where and $\Delta_{a:\flat}$ refers to a covariant derivative of Δ wrt the metric $g_{a\flat}$ on the sphere.[1] Here κ, $\gamma_{a\flat}$, and ω give the expansion, shear, and rotation. The shear is defined such that $g^{a\flat}\gamma_{a\flat} = 0$ which fully specifies κ. From the shear field one may define two new quantities

$$\gamma_{\rm s} = \nabla^{-2}\gamma_{a\flat}{}^{:a\flat} \qquad \gamma_{\rm p} = \nabla^{-2}\gamma_{a\flat}{}^{:b c}\epsilon^{a}{}_{c}. \tag{4.2}$$

where ∇^{-2} is the inverse Laplace operator on the sphere, i.e.

$$\nabla^2\phi \equiv \phi_{:a}{}^{a} \qquad \nabla^{-2}\phi_{:a}{}^{a} = \phi + \text{constant}. \tag{4.3}$$

We must add the arbitrary constant because the ∇^{-2} is not completely defined since ∇^2 has a zero eigenvalue which corresponds to the constant, $l = 0$, eigenmode. Here l gives the eigenvalue of the Laplace operator which is $-l(l+1)$. The quantity $\gamma_{\rm s}$ is contributed to only by the scalar part of the shear, as described in §2, while the quantity $\gamma_{\rm p}$ is contributed only to by the pseudo-scalar part of the shear. From $\gamma_{\rm s}$ and $\gamma_{\rm p}$ one can fully reconstruct $\gamma_{a\flat}$. However from $\gamma_{a\flat}$ or from $\gamma_{\rm s}$ and $\gamma_{\rm p}$, one cannot, in general, fully reconstruct the displacement vector $\vec{\Delta}$. As we shall see, the $l = 1$ eigenmodes do effect Δ but not $\gamma_{a\flat}$. The fact that the $l = 0$ eigenmodes also do not contribute to $\gamma_{a\flat}$ does not matter since it also does not contribute to $\vec{\Delta}$. By definition κ and ω have zero mean and therefore no contribution from the $l = 0$ eigenmode. It therefore makes since to define $\gamma_{\rm s}$ and $\gamma_{\rm p}$ to have zero mean and therefore no contribution for the $l = 0$ eigenmode. By construction they have not contribution from the $l = 1$ eigenmodes.

Above we have used the completely antisymmetric tensor defined by

$$\epsilon_{a\flat} = \sqrt{g}\begin{pmatrix} 0 & 1 \\ -1 & 0 \end{pmatrix} \qquad \epsilon^{a}{}_{\flat} = \frac{1}{\sqrt{g}}\begin{pmatrix} g_{12} & g_{22} \\ -g_{11} & -g_{21} \end{pmatrix} \qquad \epsilon^{a\flat} = \frac{1}{\sqrt{g}}\begin{pmatrix} 0 & 1 \\ -1 & 0 \end{pmatrix} \qquad g \equiv \|g_{a\flat}\| \tag{4.4}$$

which commutes with covariant differentiation, i.e. $\epsilon^{a\flat}{}_{:c} = 0$. When $\epsilon_{a\flat}$ is contracted with a 1-index vector it has the effect of rotating the vector by 90°. Whether the rotation is to the left of right can be chosen arbitrarily, but whatever choice one makes the sign of $\epsilon_{a\flat}$ is multiplied by -1 under a parity transformation, and thus a leftward rotation is transformed to a rightward and vice-versa. Thus quantities containing odd numbers of $\epsilon_{a\flat}$'s are odd under parity and we refer to them a pseudo-scalar part of the shear. Note also that the shear $\epsilon_{a}{}^{2}{}_{b}\gamma_{a\flat}$ yields another traceless symmetric tensor which if interpreted as a shear tensor has it's shear rotated by 45° wrt that of the original shear tensors. Rotating the displacement vectors by 90° corresponds to rotating the shear by 45°. Performing either of these rotations will transform a purely scalar patter to a purely pseudo-scalar one, and vice-versa.

[1] All of the indexed quantities are components of tensors on the sphere. Below we will use the coordinate bases defined by spherical polar coordinates, (θ, ϕ) on the sphere. Although the two basis vector are orthogonal they are not orthonormal, and in particular, tensor components with a ϕ index will contain extra factors of $\sin^2\theta$ when compared to tensors defined with respect to an orthonormal basis in the same direction.

Spherical Harmonic Expansion

In analogy with the Fourier expansion of §2 we may expand the displacement vector on the sphere in terms of a spherical harmonic functions $Y_{(l,m)}(\hat{\mathbf{n}})$. These functions are defined such that

$$\nabla^2 Y_{(l,m)}(\hat{\mathbf{n}}) = -l(l+1)Y_{(l,m)}(\hat{\mathbf{n}}) \qquad \int d^2\hat{\mathbf{n}}\, Y_{(l,m)}\, Y^*_{(l',m')} = \delta_{ll'}\delta_{mm'}. \tag{4.5}$$

Using 2-d spherical geometry this implies the identities

$$\begin{aligned} Y_{(l,m)}{}^{:ab}{}_{:ab} &= \nabla^2\nabla^2 Y_{(l,m)} + \nabla^2 Y_{(l,m)} = l\,(l+1)\,(l(l+1)-1)\,Y_{(l,m)} \\ \int d^2\hat{\mathbf{n}}\, Y_{(l,m):ab}\, Y^{*}_{(l',m')}{}^{:ab} &= l\,(l+1)\,(l(l+1)-1)\,\delta_{ll'}\delta_{mm'} \end{aligned} \tag{4.6}$$

The spherical harmonic analog of eq (2.5) is

$$\Delta_a = -\sum_{l=1}^{\infty}\sum_{m=-l}^{+l}\left(\phi^{\oplus}_{(l,m)} Y_{(l,m):a} + \phi^{\otimes}_{(l,m)} Y_{(l,m):b}\epsilon^{b}{}_{a}\right) \tag{4.7}$$

including both scalar and pseudo-scalar displacement. Note that we do not include a $l = m = 0$ term in the sum since $Y_{(0,0):a} = 0$. Furthermore since Δ_a is real we require

$$\phi^{\oplus}_{(l,m)} = (-1)^m \phi^{\oplus}_{(l,m)}{}^{*} \qquad \phi^{\otimes}_{(l,m)} = (-1)^m \phi^{\otimes}_{(l,m)}{}^{*} \qquad \text{since} \qquad Y^*_{(l,-m)} = (-1)^m Y_{(l,m)}. \tag{4.8}$$

In the above decomposition the $\phi^{\oplus}_{(l,m)}$ terms give the scalar part of the displacement vector which is proportional to the gradient of the spherical harmonic, $Y_{(l,m)}$. The pseudo-scalar part, given by the $\phi^{\otimes}$ terms, is proportional to the gradient of $Y_{(l,m)}$ rotated by 90°. The deformation tensor is then given by

$$\psi_{ab} = g_{ab} - \sum_{l=1}^{\infty}\sum_{m=-l}^{+l}\left(\phi^{\oplus}_{(l,m)} Y_{(l,m):ab} + \phi^{\otimes}_{(l,m)} Y_{(l,m):ac}\epsilon^{c}{}_{b}\right) \tag{4.9}$$

and it's component parts by

$$\begin{aligned} \kappa &= -\frac{1}{2}\sum_{l=1}^{\infty}\sum_{m=-l}^{+l} l(l+1)\phi^{\oplus}_{(l,m)} Y_{(l,m)} \\ \omega &= -\frac{1}{2}\sum_{l=1}^{\infty}\sum_{m=-l}^{+l} l(l+1)\phi^{\otimes}_{(l,m)} Y_{(l,m)} \\ \gamma_{ab} &= \sum_{l=2}^{\infty}\sum_{m=-l}^{+l}\left(\phi^{\oplus}_{(l,m)}\left(Y_{(l,m):ab} - \frac{1}{2}g_{ab}Y_{(l,m):c}{}^{:c}\right) + \phi^{\otimes}_{(l,m)}\frac{1}{2}\left(Y_{(l,m):ac}\epsilon^{c}{}_{b} + Y_{(l,m):bc}\epsilon^{c}{}_{a}\right)\right) \end{aligned} \tag{4.10}$$

where we have used eq (4.5). In the shear we do not include the $l = 1$ terms, since the deformation tensor from these modes do not contribute to the shear as we will see below. Combining (4.2,6,&10) one finds

$$\begin{aligned} \gamma_s &= (-\nabla^{-2}\psi_{ab}{}^{:ab} + \kappa) = \frac{1}{2}\sum_{l=2}^{\infty}\sum_{m=-l}^{+l}(l+2)(l-1)\,\phi^{\oplus}_{(l,m)}\,Y_{(l,m)} \\ \gamma_p &= -(\nabla^{-2}\psi_{ab}{}^{:bc}\epsilon^{a}{}_{c} - \nabla^{-2}(\omega\epsilon_{ab})^{:bc}\epsilon^{a}{}_{c}) = \frac{1}{2}\sum_{l=1}^{\infty}\sum_{m=-l}^{+l}(l+2)(l-1)\,\phi^{\otimes}_{(l,m)}\,Y_{(l,m)} \end{aligned} \tag{4.11}$$

and that the $l = 1$ terms do not contribute to either γ_s or γ_p. For large l we recover the small angle result, i.e. $\gamma_s = \kappa$ and $\gamma_p = -\omega$. These relations hold for any deformation of our sky onto the 3-d space, but they are nevertheless they are non-trivial consistency checks. For example one can hope to measure both γ_s and κ, the former from galaxy alignments and the later from galaxy brightness distributions in various bands. These being independent measures of the same thing would provide a consistency check. If they were found to be inconsistent then would discover that one is not measuring variations in alignments and brightnesses due to an image deformation. Measurement error, Galactic extinction, intrinsic alignments, intrinsic galaxy clusterings and other effects will all contribute to inconsistencies.

Decomposition of Distortion Pattern

Given combinations of Δ^a, κ, ω, γ_s, γ_p, or γ^{ab} one can compute the mode coefficients via

$$\begin{aligned}
\phi^{\oplus}_{(l,m)} &= -\frac{1}{l(l+1)}\int d^2\hat{\mathbf{n}}\, Y^*_{(l,m);a}\,\Delta^a = +\frac{1}{l(l+1)}\int d^2\hat{\mathbf{n}}\, Y^*_{(l,m)}\,\Delta^a{}_{;a} = -\frac{2}{l(l+1)}\int d^2\hat{\mathbf{n}}\, Y^*_{(l,m)}\,\kappa \\
\phi^{\otimes}_{(l,m)} &= +\frac{1}{l(l+1)}\int d^2\hat{\mathbf{n}}\, Y^*_{(l,m);a}\,\Delta^b\epsilon^a{}_b = -\frac{1}{l(l+1)}\int d^2\hat{\mathbf{n}}\, Y^*_{(l,m)}\,\Delta^b{}_{;a}\epsilon^a{}_b = \frac{2}{l(l+1)}\int d^2\hat{\mathbf{n}}\, Y^*_{(l,m)}\,\omega \\
\phi^{\oplus}_{(l,m)} &= +\frac{1}{l(l+1)(l(l+1)-1)}\int d^2\hat{\mathbf{n}}\, Y^*_{(l,m);ab}\,\psi^{ab} = \frac{1}{l(l+1)-1}\int d^2\hat{\mathbf{n}}\, Y^*_{(l,m)}\,(\gamma_s+\kappa) \\
\phi^{\otimes}_{(l,m)} &= +\frac{1}{l(l+1)(l(l+1)-1)}\int d^2\hat{\mathbf{n}}\, Y^*_{(l,m);ac}\,\epsilon^c{}_b\,\psi^{ab} = \frac{1}{l(l+1)-1}\int d^2\hat{\mathbf{n}}\, Y^*_{(l,m)}\,(\gamma_p-\omega) \\
\phi^{\oplus}_{(l,m)} &= +\frac{2}{(l+2)(l+1)l(l-1)}\int d^2\hat{\mathbf{n}}\, Y^*_{(l,m);ab}\,\gamma^{ab} = -\frac{2}{(l+2)(l-1)}\int d^2\hat{\mathbf{n}}\, Y^*_{(l,m)}\,\gamma_s \\
\phi^{\otimes}_{(l,m)} &= +\frac{2}{(l+2)(l+1)l(l-1)}\int d^2\hat{\mathbf{n}}\, Y^*_{(l,m);ac}\,\epsilon^{cd}\gamma^{ad} = -\frac{2}{(l+2)(l-1)}\int d^2\hat{\mathbf{n}}\, Y^*_{(l,m)}\,\gamma_p
\end{aligned} \tag{4.12}$$

using the orthonormality relation of eqs (4.5&6). We see that one cannot obtain the $l=1$ terms from the shear since substituting $l=1$ in the last four expressions one finds that the prefactors are infinite while the integrals are zero.

Mean Square Expansion, Rotation, and Shear

For a given realization of the shear pattern one can construct the quantities

$$\widehat{C^{\oplus}_l} = \frac{l^2(l+1)^2}{4(2l+1)}\sum_{m=-l}^{l}|\phi^{\oplus}_{(l,m)}|^2 \qquad \widehat{C^{\otimes}_l} = \frac{l^2(l+1)^2}{4(2l+1)}\sum_{m=-l}^{l}|\phi^{\otimes}_{(l,m)}|^2. \tag{4.13}$$

The $\widehat{\ }$ notation is used to indicate that these quantities may be used as estimators of the power spectra coefficients, $C^{\oplus}_l$ and $C^{\otimes}_l$, defined below. Combining the decomposition in eq (4.10) with the orthonormality relations of eqs (4.5&6) we find that the mean square κ, ω, and γ_{ab} averaged over the sky is

$$\begin{aligned}
\overline{\kappa^2} &= \sum_{l=1}^{\infty}\frac{2l+1}{4\pi}\widehat{C^{\oplus}_l} \\
\overline{\omega^2} &= \sum_{l=1}^{\infty}\frac{2l+1}{4\pi}\widehat{C^{\otimes}_l} \\
\overline{\gamma^2} = \overline{-||\gamma^a{}_b||} &= \frac{1}{2}\overline{\gamma^{ab}\gamma_{ab}} = \sum_{l=2}^{\infty}\frac{2l+1}{4\pi}\,\frac{(l+2)(l-1)}{l(l+1)}\,(\widehat{C^{\oplus}_l}+\widehat{C^{\otimes}_l})
\end{aligned} \tag{4.14}$$

where $||\gamma^a{}_b||$ indicates the determinant of the matrix $\gamma^a{}_b$. We use the notation $\bar{}$ to indicate averages over the sky. One expects the mean square shear to receive it's largest contribution from small angular scale so that the large l terms dominate these sums. If this is the case then $\overline{\gamma^2} \approx \overline{\kappa^2} + \overline{\omega^2}$. One could construct equations analogous to eq (4.14) for mean-square values after convolution with a window function by one could include a $|W_l|^2$ factor to each of the terms of the sum, where W_l is the spherical harmonic decomposition of the window function.

Explicit Construction of the Shear Tensor

Here we give the explicit expression for the shear tensor in terms of the spherical harmonic mode coefficients. Using spherical polar coordinates, (θ,ϕ), the metric and anti-symmetric tensor are

$$g_{ab} = \begin{pmatrix} 1 & 0 \\ 0 & \sin^2\theta \end{pmatrix} \qquad g = \sin^2\theta \qquad \epsilon^a{}_b = \begin{pmatrix} 0 & \sin\theta \\ -\frac{1}{\sin\theta} & 0 \end{pmatrix} \tag{4.15}$$

so (4.10) becomes

$$\gamma_{ab} = +\sum_{l=2}^{\infty}\sum_{m=-l}^{+l}\phi^{\oplus}_{(l,m)}\begin{pmatrix} \frac{1}{2}Y_{(l,m):\theta\theta} - \frac{1}{2\sin^2\theta}Y_{(l,m):\phi\phi} & Y_{(l,m):\theta\phi} \\ Y_{(l,m):\theta\phi} & \frac{1}{2}Y_{(l,m):\phi\phi} - \frac{1}{2}\sin^2\theta\, Y_{(l,m):\theta\theta}\end{pmatrix} + \sum_{l=2}^{\infty}\sum_{m=-l}^{+l}\phi^{\otimes}_{(l,m)}\begin{pmatrix} -\frac{1}{\sin\theta}Y_{(l,m):\theta\phi} & \frac{1}{2}\sin\theta\, Y_{(l,m):\theta\theta} - \frac{1}{2\sin\theta}Y_{(l,m):\phi\phi} \\ \frac{1}{2}\sin\theta\, Y_{(l,m):\theta\theta} - \frac{1}{2\sin\theta}Y_{(l,m):\phi\phi} & \sin\theta\, Y_{(l,m):\theta\phi}\end{pmatrix} \tag{4.16}$$

To continue we need the explicit form of the spherical harmonics, which we take to be

$$Y_{(l,m)}(\theta,\phi) = \sqrt{\frac{2l+1}{4\pi}\frac{(l-m)!}{(l+m)!}}\,P_l^m(\cos\theta)\,e^{im\phi} \tag{4.17}$$

following the conventions of Jackson (1975).

Using this explicit form of the spherical harmonics one can show that the deflection vectors $Y_{(1,0):b}\epsilon^b{}_a$, $(Y_{(1,+1):b} + Y_{(1,-1):b})\epsilon^b{}_a$, and $i(Y_{(1,+1):b} - Y_{(1,-1):b})\epsilon^b{}_a$, are generators of solid body rotations of the sphere. Clearly solid body rotation generates no amplification or shear, but does translate and/or rotate the images and thus we see why the $l = 1$ pseudo-scalar displacement contributes nothing to the shear, γ_{ab}. The $l = 1$ scalar displacement is just the pseudo-scalar displacement rotated by 90° which would yield a shear rotated by 45°. However since the $l = 1$ pseudo-scalar shear is zero, so must be the $l = 1$ scalar shear.

Let us defining two auxiliary function via

$$\begin{aligned}\sqrt{\frac{2l+1}{4\pi}\frac{(l-m)!}{(l+m)!}}\,G^{+}_{(l,m)}(\cos\theta)\,e^{im\phi} &= \frac{1}{2}Y_{(l,m):\theta\theta} - \frac{1}{2\sin^2\theta}Y_{(l,m):\phi\phi} \\ \sqrt{\frac{2l+1}{4\pi}\frac{(l-m)!}{(l+m)!}}\,G^{-}_{(l,m)}(\cos\theta)\,e^{im\phi} &= Y_{(l,m):\theta\phi}\end{aligned} \tag{4.18}$$

or more explicitly

$$\begin{aligned}G^{+}_{(l,m)}(x) &= -\left(\frac{l-m^2}{1-x^2} + \frac{1}{2}l(l-1)\right)P_l^m(x) + (l+m)\frac{x}{1-x^2}P_{l-1}^m(x) \\ G^{-}_{(l,m)}(x) &= m\left((l-1)\frac{x}{1-x^2}P_l^m(x) - (l+m)\frac{1}{1-x^2}P_{l-1}^m(x)\right)\end{aligned} \tag{4.19}$$

we find from substituting (4.18) into (4.16) that

$$\begin{aligned}\gamma_{\theta\theta} = -\frac{\gamma_{\phi\phi}}{\sin^2\theta} &= \sum_{l=2}^{\infty}\sqrt{\frac{2l+1}{4\pi}}\sum_{m=-l}^{+l}\sqrt{\frac{(l-m)!}{(l+m)!}}\left(\phi^{\oplus}_{(l,m)}\,G^{+}_{(l,m)}(\cos\theta) - i\phi^{\otimes}_{(l,m)}\,G^{-}_{(l,m)}(\cos\theta)\right)e^{im\phi} \\ \frac{\gamma_{\theta\phi}}{\sin\theta} = \frac{\gamma_{\phi\theta}}{\sin\theta} &= \sum_{l=2}^{\infty}\sqrt{\frac{2l+1}{4\pi}}\sum_{m=-l}^{+l}\sqrt{\frac{(l-m)!}{(l+m)!}}\left(i\phi^{\oplus}_{(l,m)}\,G^{-}_{(l,m)}(\cos\theta) + \phi^{\otimes}_{(l,m)}\,G^{+}_{(l,m)}(\cos\theta)\right)e^{im\phi}\end{aligned} \tag{4.20}$$

Note the symmetry relations

$$G^{\pm}_{(l,-m)} = \pm(-1)^m\frac{(l+m)!}{(l-m)!}\,G^{\pm}_{(l,m)} \tag{4.21}$$

and the orthonormality relations

$$\begin{aligned}\frac{1}{2}\int_{-1}^{1}dx\,(G^{+}_{(l,m)}(x)\,G^{+}_{(l',m)}(x) + G^{-}_{(l,m)}(x)\,G^{-}_{(l',m)}(x)) &= \frac{1}{4(2l+1)}\frac{(l+2)!}{(l-2)!}\frac{(l+m)!}{(l-m)!}\delta_{ll'} \\ \frac{1}{2}\int_{-1}^{1}dx\,(G^{+}_{(l,m)}(x)\,G^{-}_{(l',m)}(x) + G^{-}_{(l,m)}(x)\,G^{+}_{(l',m)}(x)) &= 0\end{aligned} \tag{4.22}$$

From these identities one can rederive the formula for $\overline{\gamma^2}$ in eq (4.14).

Below we will find that it is of particular interest to calculate the shear at the pole of the coordinate system. In spite of the fact that the coordinates system is singular at the pole, mode expansion at the pole takes a particularly simple form. The coordinate singularity means that one should consider only $\gamma_{\theta\theta}$ in the limit $\theta \to 0$ for a given value of ϕ. In this limit the value $\gamma_{\theta\theta}$ will retain an ϕ-dependence and from this one has the angular dependence of the shear. One finds that in the $\theta = 0$ limit that only $m = \pm 2$ contributes

$$G^{\pm}_{(l,m)}(1) = \frac{1}{4}\frac{(l+2)!}{(l-2)!}\delta_{m,2} \pm \frac{1}{4}\delta_{m,-2} \tag{4.23}$$

which on can use to compute the 2-point correlation function of the shear.

Correlation Functions and Power Spectrum

Henceforth we shall explicitly include the radial r-dependence of the deformation since we may be interested in correlating the different components of the correlation at different redshifts. We shall also be considering a statistical distribution of deformation fields. Averaging over realizations, one can characterize any set of 2-point functions in terms of the power spectra which we choose to define by

$$\left\langle \phi^{\oplus}_{(l,m)}(r)\, \phi^{\oplus}_{(l',m')}{}^{*}(r') \right\rangle = \frac{4C^{\oplus}_l(r,r')}{l^2(l+1)^2}\delta_{ll'}\delta_{mm'} \qquad \left\langle \phi^{\otimes}_{(l,m)}(r)\, \phi^{\otimes}_{(l',m')}{}^{*}(r') \right\rangle = \frac{4C^{\otimes}_l(r,r')}{l^2(l+1)^2}\delta_{ll'}\delta_{mm'}. \tag{4.24}$$

The Kronecker δ-functions and the lack of m-dependence follow from the assumed homogeneity and isotropy of the distributions we are considering. We include a dependence of the deformation with depth r. We will also assume that the distribution of deformations is even under parity as it would be for gravitationally induced deformations. Since $\phi^{\oplus}$ is even under parity and $\phi^{\otimes}$ is odd under parity it follows that

$$\left\langle \phi^{\oplus}_{(l,m)}(r)\phi^{\otimes}_{(l',m')}{}^{*}(r') \right\rangle = 0. \tag{4.25}$$

Both $C^{\oplus}_l(r,r')$ and $C^{\otimes}_l(r,r')$ are real and are non-negative when $r = r'$.

The correlation functions of various quantities can be computed in terms of the correlation function

$$\begin{aligned}
C_\kappa(r,r',\vartheta) &= \langle \kappa(r,\hat{\mathbf{n}})\,\kappa(r',\hat{\mathbf{n}}')\rangle = \frac{1}{4\pi}\sum_{l=1}^{\infty}(2l+1)\,P_l(\cos\vartheta)\,C^{\oplus}_l(r,r') \\
C_\omega(r,r',\vartheta) &= \langle \omega(r,\hat{\mathbf{n}})\,\omega(r',\hat{\mathbf{n}}')\rangle = \frac{1}{4\pi}\sum_{l=1}^{\infty}(2l+1)\,P_l(\cos\vartheta)\,C^{\otimes}_l(r,r') \\
\langle \kappa(r,\hat{\mathbf{n}})\,\omega(r',\hat{\mathbf{n}}')\rangle &= 0 \\
C_\gamma(r,r',\vartheta,\varphi,\varphi') &= \frac{1}{2\pi}\sum_{l=2}^{\infty}\frac{2l+1}{l^2(l+1)^2}\Big[(C^{\oplus}_l(r,r')\,G^{+}_{(l,2)}(\cos\vartheta) + C^{\otimes}_l(r,r')\,G^{-}_{(l,2)}(\cos\vartheta))\,\cos 2\varphi\,\cos 2\varphi' \\
&\qquad + (C^{\oplus}_l(r,r')\,G^{-}_{(l,2)}(\cos\vartheta) + C^{\otimes}_l(r,r')\,G^{+}_{(l,2)}(\cos\vartheta))\,\sin 2\varphi\,\sin 2\varphi'\Big] \\
C_{\gamma\kappa}(r,r',\vartheta,\varphi) &= -\frac{1}{4\pi}\sum_{l=2}^{\infty}\frac{2l+1}{l(l+1)}\,C^{\oplus}_l(r,r')\,P^2_l(\cos\vartheta)\,\cos 2\varphi \\
C_{\gamma\omega}(r,r',\vartheta,\varphi) &= +\frac{1}{4\pi}\sum_{l=2}^{\infty}\frac{2l+1}{l(l+1)}\,C^{\otimes}_l(r,r')\,P^2_l(\cos\vartheta)\,\sin 2\varphi
\end{aligned} \tag{4.26}$$

In each of the above expressions $\vartheta = \angle(\hat{\mathbf{n}},\hat{\mathbf{n}}')$, i.e. the angle between the two points. C_γ measures the correlation of γ_{ab} with itself, while $C_{\gamma\kappa}$ and $C_{\gamma\omega}$ measures the correlation of γ_{ab} with κ and ω, respectively. The meaning of φ and φ' are described in fig 2. Setting $C^{\otimes}_l = 0$ in C_γ we obtain a correlation function similar to those in Kaiser (1993). The $C_{++}(\alpha)$, $C_{+\times}(\alpha)$, and $C_{\times\times}(\alpha)$ of that paper corresponds to setting $\varphi = \varphi' = \alpha$, $\varphi = \varphi' + \frac{\pi}{4} = \alpha$, $\varphi = \varphi' = \alpha - \frac{\pi}{4}$. Kaiser (1992) paper did not include pseudo-scalar shear since this is not contributed to by density perturbations.

From the above correlation function one may calculate the the mean square quantities at a given distance

$$\langle\kappa^2\rangle = C_\kappa(r,r,0) = \sum_{l=1}^{\infty} \frac{2l+1}{4\pi} C_l^{\oplus}(r,r) \qquad \langle\omega^2\rangle = C_\omega(r,r,0) = \sum_{l=1}^{\infty} \frac{2l+1}{4\pi} C_l^{\otimes}(r,r)$$
$$\langle\gamma^2\rangle = \langle\frac{1}{2}\gamma^{ab}\gamma_{ab}\rangle = C_\gamma(r,r,\vartheta,0,0) + C_\gamma(r,r,\vartheta,\frac{\pi}{4},\frac{\pi}{4}) = \sum_{l=2}^{\infty} \frac{2l+1}{4\pi} \frac{(l+2)(l-1)}{l(l+1)} \left[C_l^{\oplus}(r,r) + C_l^{\otimes}(r,r)\right] \tag{4.27}$$

Note that the factor $(l+2)(l-1)/(l(l+1)) = 1 + \mathcal{O}(l^{-2})$, and since most of the shear is expected to be generated at very small scales we find

$$\langle\gamma^2\rangle \approx \langle\kappa^2\rangle + \langle\omega^2\rangle. \tag{4.28}$$

Remember that although (4.14) is quite similar to (4.27) the former refers to averages over the sphere for a given realization, which could be a observed quantity, while the latter refers to an average over realization and is a purely theoretical construct. The reasons that the formulae are so similar is because, by construction,

$$\langle\widehat{C_l^{\oplus}}(r,r')\rangle = C_l^{\oplus}(r,r') \qquad \langle\widehat{C_l^{\otimes}}(r,r')\rangle = C_l^{\otimes}(r,r'), \tag{4.29}$$

i.e $\widehat{C_l^{\oplus}}$ and $\widehat{C_l^{\otimes}}$ are unbiased estimators of $C_l^{\oplus}$ and $C_l^{\otimes}$, respectively.

Comparing (4.26) with the orthonormality relations, (4.5&6) as well as

$$\frac{1}{2}\int_{-1}^{1} dx\, P_l(x)\, P_{l'}(x) = \frac{1}{2l+1}\delta_{ll'} \tag{4.30}$$

we see that if one knows the correlation functions one may calculate the power spectra using

$$\begin{aligned}
C_l^{\oplus}(r,r') =& 2\pi\int_{-1}^{1} dx\, P_l(x)\, C_\kappa(r,r'\cos^{-1}x) = -\frac{2}{(l+2)(l-1)}\int_{-1}^{1} dx \int_0^{2\pi} d\varphi\, P_l^2(x)\, C_{\gamma\kappa}(r,r',\cos^{-1}x,\varphi)\cos 2\phi \\
C_l^{\otimes}(r,r') =& 2\pi\int_{-1}^{1} dx\, P_l(x)\, C_\omega(r,r'\cos^{-1}x) = -\frac{2}{(l+2)(l-1)}\int_{-1}^{1} dx \int_0^{2\pi} d\varphi\, P_l^2(x)\, C_{\gamma\omega}(r,r',\cos^{-1}x,\varphi)\sin 2\phi \\
C_l^{\oplus}(r,r') =& \frac{4}{\pi}\frac{1}{(l+2)^2(l-1)^2}\int_{-1}^{1} dx \int_0^{2\pi} d\varphi \int_0^{2\pi} d\varphi'\, C_\gamma(r,r',\cos^{-1}x,\varphi,\varphi')\times \\
& \qquad \left(G_{(l,2)}^{+}(x)\cos 2\varphi\cos 2\varphi' + G_{(l,2)}^{-}(x)\sin 2\varphi\sin 2\varphi'\right) \\
C_l^{\otimes}(r,r') =& \frac{4}{\pi}\frac{1}{(l+2)^2(l-1)^2}\int_{-1}^{1} dx \int_0^{2\pi} d\varphi \int_0^{2\pi} d\varphi'\, C_\gamma(r,r',\cos^{-1}x,\varphi,\varphi')\times \\
& \qquad \left(G_{(l,2)}^{+}(x)\sin 2\varphi\sin 2\varphi' + G_{(l,2)}^{-}(x)\cos 2\varphi\cos 2\varphi'\right)
\end{aligned} \tag{4.31}$$

Small-Angle Limit

Now let us consider the small angle limit of the formulae just derived. Over small angles the surface of the sphere is approximately a plane, and the wavenumber, l, can be consider modulus of a 2-d vector wavenumber in this plane in a Fourier decomposition of the displacement if $l \gg 1$. This Fourier representation is context in which most analyses of image deformation has been analyzed, and the formulae derived above should approach this Fourier limit for $l \gg 1$ over regions much smaller than one radian. In particular the angular correlation function should approach the Fourier limit for $l \gg 1$ and $\vartheta \ll 1$. In the small-angle large-l limit one can show

$$\begin{aligned}
G_{(l,m)}^{\pm}(\cos\theta) &= (-1)^m \frac{1}{4} l^{6-m}(J_{m-2}(l\theta) \pm J_{m+2}(l\theta)) + \mathcal{O}(\frac{1}{l},\frac{m}{l},\theta^2) \\
P_l^m(\cos\theta) &= (-1)^m \frac{(l+m)!}{(l-m)!} J_m(l\theta) l^{-m} + \mathcal{O}(\frac{1}{l^{m+2}},\frac{m}{l},\theta^2)
\end{aligned} \tag{4.32}$$

Thus in the small-angle approximation the correlation functions become

$$\begin{aligned}
C_\kappa(r,r',\vartheta) &\approx \frac{1}{2\pi}\int^\infty dl\, l\, J_0(l\vartheta)\, C_l^\oplus(r,r') \qquad C_{\gamma\kappa}(r,r',\vartheta,\varphi) \approx -\frac{1}{2\pi}\int^\infty dl\, l\, J_2(l\vartheta)\, C_l^\oplus(r,r')\, \cos 2\varphi \\
C_\omega(r,r',\vartheta) &\approx \frac{1}{2\pi}\int^\infty dl\, l\, J_0(l\vartheta)\, C_l^\otimes(r,r') \qquad C_{\gamma\omega}(r,r',\vartheta,\varphi) \approx +\frac{1}{2\pi}\int^\infty dl\, l\, J_2(l\vartheta)\, C_l^\otimes(r,r')\, \sin 2\varphi \\
C_\gamma(r,r',\vartheta,\varphi,\varphi') &\approx \frac{1}{4\pi}\int^\infty dl\, l \Big[(C_l^\oplus(r,r')\,(J_0(l\vartheta)+J_4(l\vartheta)) + C_l^\otimes(r,r')\,(J_0(l\vartheta)-J_4(l\vartheta)))\, \cos 2\varphi \cos 2\varphi' \\
&\qquad + (C_l^\oplus(r,r')\,(J_0(l\vartheta)-J_4(l\vartheta)) + C_l^\otimes(r,r')\,(J_0(l\vartheta)+J_4(l\vartheta)))\, \sin 2\varphi \sin 2\varphi' \Big]
\end{aligned} \tag{4.33}$$

while the small angle limit of (4.31) is

$$\begin{aligned}
C_l^\oplus(r,r') &\approx 2\pi \int_0^\infty d\vartheta\, \vartheta\, J_0(l\vartheta)\, C_\kappa(r,r'\vartheta) \approx -2\int_0^\infty d\vartheta\, \vartheta \int_0^{2\pi} d\varphi\, J_2(l\vartheta)\, C_{\gamma\kappa}(r,r',\vartheta,\varphi)\, \cos 2\phi \\
C_l^\otimes(r,r') &\approx 2\pi \int_0^\infty d\vartheta\, \vartheta\, J_0(l\vartheta)\, C_\omega(r,r'\vartheta) \approx -2\int_0^\infty d\vartheta\, \vartheta \int_0^{2\pi} d\varphi\, J_2(l\vartheta)\, C_{\gamma\omega}(r,r',\vartheta,\varphi)\, \sin 2\phi \\
C_l^\oplus(r,r') &\approx \frac{1}{\pi}\int_0^\infty d\vartheta\, \vartheta \int_0^{2\pi} d\varphi \int_0^{2\pi} d\varphi'\, C_\gamma(r,r',\vartheta,\varphi,\varphi')\,(J_0(l\vartheta)\, \cos 2(\varphi-\varphi') + J_4(l\vartheta)\, \cos 2(\varphi+\varphi')) \\
C_l^\otimes(r,r') &\approx \frac{1}{\pi}\int_0^\infty d\vartheta\, \vartheta \int_0^{2\pi} d\varphi \int_0^{2\pi} d\varphi'\, C_\gamma(r,r',\vartheta,\varphi,\varphi')\,(J_0(l\vartheta)\, \cos 2(\varphi-\varphi') - J_4(l\vartheta)\, \cos 2(\varphi+\varphi'))
\end{aligned} \tag{4.34}$$

Using a 2-d definition of a power spectrum where

$$\langle f(\hat{\mathbf{n}})\, f(\hat{\mathbf{n}}')\rangle = 2\pi \int_0^\infty dl\, l\, P_f(l)\, J_0(l\vartheta) \qquad \vartheta = \angle(\hat{\mathbf{n}},\hat{\mathbf{n}}') \tag{4.35}$$

we see that

$$P_\kappa(l) = \frac{1}{4\pi^2}\, C_l^\oplus \qquad P_\omega(l) = \frac{1}{4\pi^2}\, C_l^\otimes \tag{4.36}$$

and that γ_{ab} is described by these same two power spectra, e.g.

$$\langle\gamma^2\rangle \approx \langle\kappa^2\rangle + \langle\omega^2\rangle \approx 2\pi \int^\infty dl\, l\, (P_\kappa(l) + P_\omega(l)) \approx \frac{1}{2\pi}\int^\infty dl\, l\, (C_l^\oplus(l) + C_l^\otimes). \tag{4.37}$$

Visibility Functions

To measure the shear one typically looks for correlations in galaxy ellipticity orientation, and one needs enough galaxies to find the correlation in the noise generated by the random orientation of the galaxies. Usually one doesn't know the distance to the galaxies except in a statistical sense, and even if one did, one would have to sum over galaxies at different distances to obtain a significant signal. Thus the shear at a given distance is not what one measures, but rather some weighted average of the shear at different distances. We may represent this distribution of distances by a visibility function, $V(r)$, normalized so that

$$\int_0^\infty dr\, V(r) = 1, \tag{4.38}$$

so that the average expansion, rotation, and shear is

$$\overline{\kappa}(\hat{\mathbf{n}}) = \int_0^\infty dr\, V(r)\, \kappa(r,\hat{\mathbf{n}}) \qquad \overline{\omega}(\hat{\mathbf{n}}) = \int_0^\infty dr\, V(r)\, \omega(r,\hat{\mathbf{n}}) \qquad \overline{\gamma}_{ab}(\hat{\mathbf{n}}) = \int_0^\infty dr\, V(r)\, \gamma_{ab}(r,\hat{\mathbf{n}}). \tag{4.39}$$

One can apply all of the formulae derived above by replacing the quantities at fixed distance with the same quantities, averaged over distance, e.g. the mode coefficients

$$\overline{\phi}^\oplus_{(l,m)} = \int_0^\infty dr\, V(r)\, \phi^\oplus_{(l,m)}(r) \qquad \overline{\phi}^\otimes_{(l,m)} = \int_0^\infty dr\, V(r)\, \phi^\otimes_{(l,m)}(r), \tag{4.40}$$

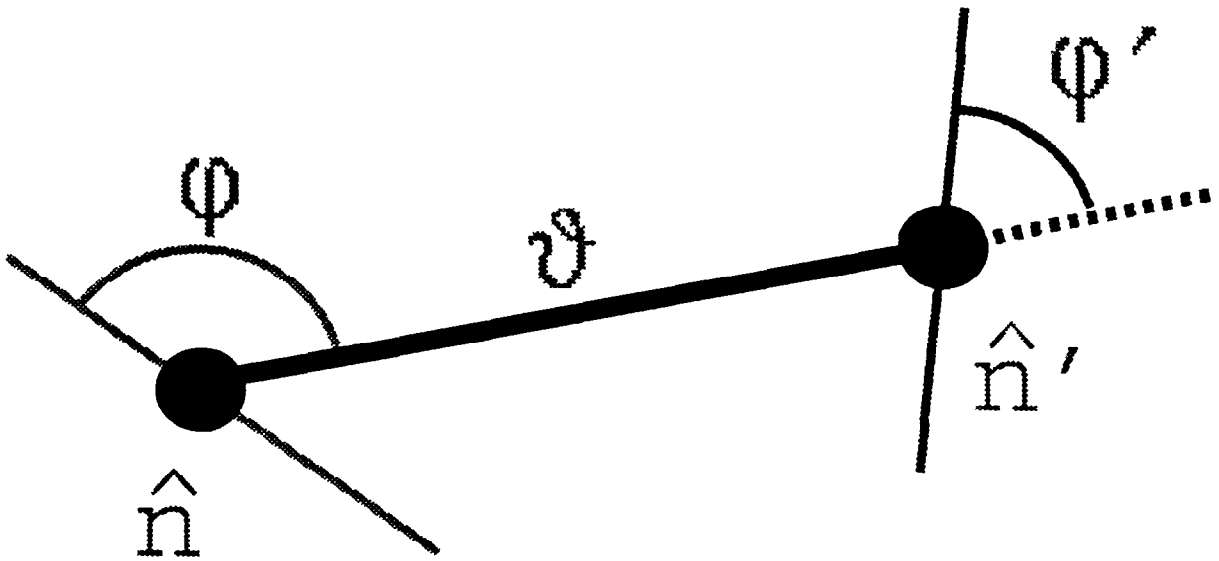

Figure 2: Here is illustrated the meaning of the variables in the 2-point correlation function C_γ, $C_{\gamma\kappa}$, and $C_{\gamma\omega}$. The thick solid line represents the geodesic connecting the two points on the celestial sphere in question, $\hat{\mathbf{n}}$ and $\hat{\mathbf{n}}'$, whose length is ϑ. The thin solid line at $\hat{\mathbf{n}}$ gives the orientation of the component of the shear that is being correlated, which is rotated φ from the direction of the geodesic. For the shear-shear correlation function, C_γ, we also need the orientation of the component of the shear at $\hat{\mathbf{n}}'$ which is given by φ'. The handedness of the coordinate system is important $C_{\gamma\omega}$ since it changes sign if $\varphi \to -\varphi$. The rotation of φ is to the right in a right-handed coordinate system. Note that the usual spherical polar coordinates, (θ, ϕ) are usually left-handed on the sky since we view the celestial sphere from the *inside*.

or the correlation functions

$$C_{\bar{x}}(\vartheta, \cdots) = \int_0^\infty dr\, V(r) \int_0^\infty dr'\, V(r')\, C_x(r, r', \vartheta, \cdots). \tag{4.41}$$

where x might be κ, ω, or γ.

It is not the purpose of this paper to be terribly realistic about how one samples the shear with a given galaxy sample. The only visibility function which we will consider explicitly in this paper corresponds to uniform sampling in space up to a given distance, $r_{\rm max}$. The visibility function in this case is

$$V(r) = 3\frac{r^2}{r_{\rm max}^3} \tag{4.42}$$

where $r_{\rm max}$ gives the maximum comoving distance which one includes in ones sample.

5. Application To Density Inhomogeneities

Here we consider the image distortion from a linear growing mode density field in a matter-dominated Einstein-deSitter cosmology. For these growing modes the Newtonian gravitational potential is constant with time at a given comoving position. It is convenient to use the Spherical Harmonic - Spherical Bessel function expansion so the

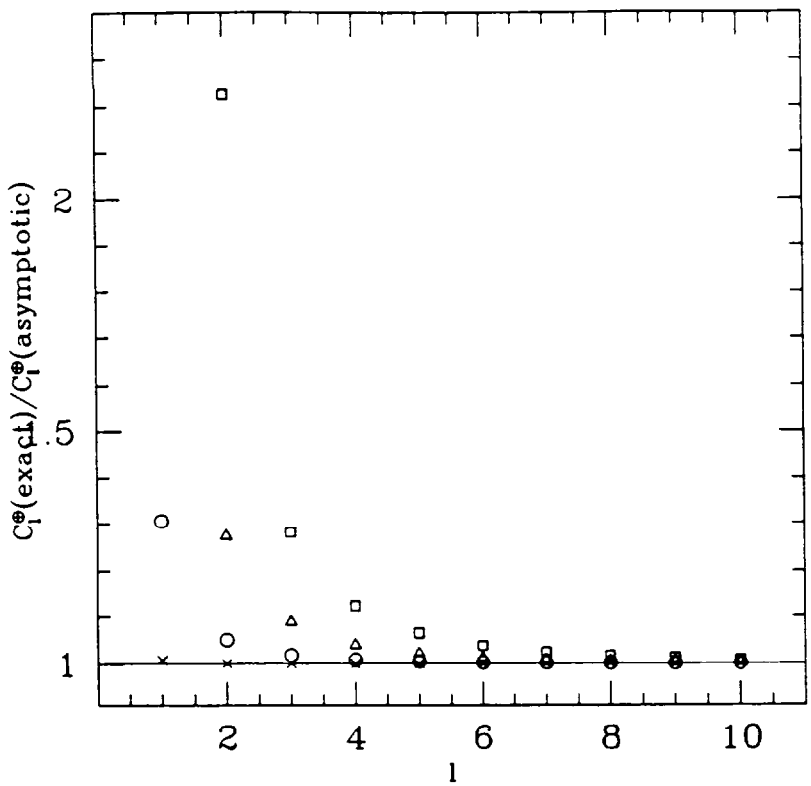

Figure 3: Plotted as a function of l, for a power law spectrum of density perturbations, is the ratio of the true $C_l^\oplus$ to that computed with the *asymptotic approximation* of eq (5.9). The power law index, n, is 0.9 for the crosses, 0 for the circles, -1 for the triangles, and -2 for the squares. The errors continue to become smaller for larger l. The ratio for $l = 1$, which contributes nothing to the shear, is not shown for $n \leq -1$ since the true value diverges for these spectral indices. The asymptotic approximation is accurate except for very small l.

gravitational potential may be expanded

$$\Phi(r,\theta,\phi) = \sum_{l=0}^{\infty}\sum_{m=-l}^{l}\int_0^\infty dk\, k^2 \widetilde{\Phi}_{(l,m)}(k)\, j_l(kr)\, Y_{(l,m)}(\theta,\phi)$$
$$\widetilde{\Phi}_{(l,m)}(k) = \frac{2}{\pi}\int_0^\infty dr\, r^2\, j_l(kr)\int_0^\pi d\theta\, \sin\theta \int_{-\pi}^{\pi} d\phi\, Y^*_{(l,m)}(\theta,\phi)\,\Phi(r,\theta,\phi) \tag{5.1}$$

where r is the comoving distance from the observer. For the spatially flat geometry we are considering, these modes are orthogonal eigenfunctions of the Laplace operator. For an statistically homogeneous and isotropic distribution the correlation function of mode amplitudes is of the form

$$\langle \widetilde{\Phi}_{(l,m)}(k)\, \widetilde{\Phi}^*_{(l',m')}(k')\rangle = (4\pi)^2 P_\Phi(k)\,\frac{1}{k^2}\,\delta(k-k')\,\delta_{ll'}\,\delta_{mm'} \tag{5.2}$$

where P_Φ is the power spectrum of the potential fluctuations. Using the relation between the potential and overdensity,

$$\nabla^2\Phi = 4\pi a^2 G\delta\rho = \frac{3}{2}\frac{H_0^2}{a^2}\delta, \tag{5.3}$$

we may also relate the potential power spectrum to the density power spectrum:

$$P_\Phi(k) = \frac{9}{4}\left(\frac{H_0}{ak}\right)^4 P_\delta(k). \tag{5.4}$$

Below we will use the notation $\hat{\mathbf{n}}$ for (θ, ϕ). Clearly these scalar modes will lead only to scalar components to the image deformation. Thus we may describe the deformation by a scalar function

$$\Delta_a = -\phi^{\oplus}{}_{;a} \qquad \phi^{\oplus}(\hat{\mathbf{n}}) = \sum_{l=1}^{\infty} \phi^{\oplus}_{(l,m)} Y_{(l,m)}(\hat{\mathbf{n}}) \qquad \phi^{\otimes}_{(l,m)} = 0. \tag{5.5}$$

Comparing eq (5.5) with eq (4.12) we find

$$\phi^{\oplus}(r, \hat{\mathbf{n}}) = 2 \int_{\eta_{obs}-r}^{\eta_{obs}} d\eta' \, \frac{r - (\eta_{obs} - \eta')}{r(\eta_{obs} - \eta')} \, \Phi(\mathbf{x}_{obs} + (\eta_{obs} - \eta')\, \hat{\mathbf{n}}, \eta') = 2 \int_0^r dr' \, \frac{r - r'}{rr'} \, \Phi(r', \hat{\mathbf{n}}), \tag{5.6}$$

and comparing this with (5.1) we see that

$$\phi^{\oplus}_{(l,m)}(r) = 2 \int_0^{\infty} dk\, k^2 \widetilde{\Phi}_{(l,m)}(k) \int_0^r dr' \, \frac{r - r'}{rr'} \, j_l(kr') = 2 \int_0^{\infty} dk\, k^2 \widetilde{\Phi}_{(l,m)}(k)\, I_l(kr) \tag{5.7}$$

where

$$I_l(x) = \int_0^1 \frac{dy}{y} \, (1 - y)\, j_l(xy) \qquad l > 0. \tag{5.8}$$

There is no need for an $l = 0$ term since there is no $l = 0$ contribution to shear or expansion. In the appendix we present analytic expressions for $I_l(x)$ as well as series and asymptotic expansions. We will argue below that in most practical applications I_l is well approximated by eq (A6), i.e.

$$I_l(x) \approx \left(a_l - \frac{b_l}{x}\right) \mathcal{H}(x - \frac{b_l}{a_l}) \qquad a_l = \frac{\sqrt{\pi}}{2l} \frac{\Gamma(\frac{l+2}{2})}{\Gamma(\frac{l+3}{2})} \quad b_l = \frac{\sqrt{\pi}}{l} \frac{\Gamma(\frac{l+1}{2})}{\Gamma(\frac{l}{2})} \tag{5.9}$$

which we call the ***asymptotic approximation***. Combining (4.24), (5.2), (5.4), and (5.7) we find

$$\begin{aligned} C_l^{\oplus}(r, r') &= 16\pi^2 l^2 (l+1)^2 \int_0^{\infty} dk\, k^2\, I_l(kr)\, I_l(kr')\, P_{\Phi}(k) \\ &= 36\pi^2 l^2 (l+1)^2 \left(\frac{H_0}{a}\right)^4 \int_0^{\infty} \frac{dk}{k^2}\, I_l(kr)\, I_l(kr')\, P_{\delta}(k) \end{aligned} \tag{5.10}$$

Taking into account a visibility function one finds

$$\overline{C_l^{\oplus}} = 36\pi^2 l^2 (l+1)^2 \left(\frac{H_0}{a}\right)^4 \int_0^{\infty} \frac{dk}{k^2} \, |\overline{I}_l(k)|^2 \, P_{\delta}(k) \tag{5.11}$$

where

$$\overline{I}_l(k) = \int_0^{\infty} dr\, V(r)\, I_l(kr). \tag{5.12}$$

From the asymptotic series of eqs (A4&5) we see that

$$\lim_{k \to 0} \overline{I}_l(k) = \frac{k^l \overline{r^l}}{(2l+1)!!\,(l+1)} \qquad \overline{r^l} \equiv \int_0^{\infty} dr\, V(r)\, r^l \qquad \lim_{k \to \infty} \overline{I}_l(k) = \lim_{k \to \infty} I_l(k) = \frac{\sqrt{\pi}}{2l} \frac{\Gamma(\frac{l+2}{2})}{\Gamma(\frac{l+3}{2})}, \tag{5.13}$$

i.e. $\overline{I}_l(k)$ goes grows like k^l for small k and goes to a constant for large k. Most visibility functions one might consider are peaked around a typical distance which we denote by r_*. The transition region between these two asymptotic forms of eq (5.13) occurs at $kr_* \sim l$. In general $\overline{I}_l(k)$ is a monotonically increasing function of k.

Deep Large-Angle Shear

Let us define the spectral index n by

$$n \equiv k\frac{d}{dk}P_\delta(k). \tag{5.14}$$

Comparing the asymptotic form of eq (5.11) with eq (5.13) we see that the $C_l^\oplus$ is well defined if $n < 1$ for large k and $n > 1 - 2l$ for small k. It seems likely in our own universe that $n \lesssim -1$ at large k while $n \sim 1$ for small k so there is no convergence problem.

In most cases the dominant contribution to $\overline{C_l^\oplus}$ is predominantly from wavenumbers $k \sim l/r_*$. The only exception to this rule that one is likely to encounter in practice is when one considers small l and deep samples. This arises because we expect to that on large scales the power spectrum will go to an $n = 1$ Harrison-Zel'dovich, i.e.

$$P(k) \approx Ak \qquad kr_{\rm HS} \lesssim 1. \tag{5.15}$$

The evidence for this comes only from measurements of large-angle CMBR anisotropies (Smoot *et al.* 1992). Studies of galaxy clustering have not yet reached large enough scales to see the spectrum approach $n \approx 1$. With weak lensing, if $r_*/l \gtrsim r_{\rm HS}$, we expect to probe larger scales than $r_{\rm HS}$. In this case the integral of eq (5.11) will have it's a largest contribution from the region where $n \approx 1$ and $\overline{I_l}(k)$ is approximately constant, i.e. the large k limit of $\overline{I_l}(k)$ but the small k limit of $P_\delta(k)$. And the integral will be approximated by

$$\overline{C_l^\oplus} \approx 36\pi^3\left(\frac{H_0}{a}\right)^4 A\left[\ln\frac{r_*}{lr_{\rm HS}}\right]\left(\frac{\Gamma(\frac{l+2}{2})}{\Gamma(\frac{l+1}{2})}\right)^2 \underset{l\gg 1}{\longrightarrow} 18\pi^3\left(\frac{H_0}{a}\right)^4 Al\left[\ln\frac{r_*}{lr_{\rm HS}}\right] \qquad r_* \gg lr_{\rm HS}. \tag{5.16}$$

Since the contribution to this part of the integral is only logarithmically dominant we never expect this to be an extremely accurate approximation. On the other hand the this expression is not very sensitive to $r_{\rm HS}$ or the way the power spectrum turns over from $n = 1$ at small scales. The contribution to $\overline{C_l^\oplus}$ comes from the wavenumbers in a broad range from $k \sim l/r_*$ to $k \sim 1/r_{\rm HS}$ rather than from a narrow range of wavenumbers near $k \sim l/r_*$. In our universe it is likely that the lo-l shear averaged over a depth of a gigaparsecs will receive significant contribution from scales of a few hundred megaparsecs to gigaparsecs.

Volume Limited Samples With Power Law Spectra

As an example we compute the angular power spectrum of the shear in a volume limited sample of galaxies in the case where the density power spectrum is a power law in wavenumber, i.e.

$$P(k) = Ak^n. \tag{5.17}$$

For a pure power law both $C_l^\oplus$ and $\overline{C_l^\oplus}$ have an ultra-violet (large k) divergence if $n \geq 1$ and an infrared (small k) divergence if $n + 2l \leq 1$. Combining the visibility function of (4.42) with the asymptotic approximation of eqs (A6) or (B9) one finds the approximate result

$$\begin{aligned}\overline{C_l^\oplus} &\approx 81\pi^3 2^n \frac{l^{3-n}}{(l+1)^{1-n}} \frac{(11-3n)(6-n)\Gamma(1-n)}{\Gamma(8-n)}\left(\frac{\Gamma(\frac{l}{2})}{\Gamma(\frac{l+1}{2})}\right)^{4-2n}\left(\frac{H_0}{a}\right)^4 Ar_{\rm max}^{1-n} \\ &\underset{l\gg 1}{\longrightarrow} 324\pi^3(11-3n)(6-n)\frac{\Gamma(1-n)}{\Gamma(8-n)} l^n \left(\frac{H_0}{a}\right)^4 Ar_{\rm max}^{1-n}\end{aligned} \qquad 1 - 2l < n < 1. \tag{5.18}$$

We illustrate that the error in this approximate result is small in fig 2. We see that for $n \lesssim 1$ eq (5.18) is an excellent approximation for all l while for smaller n there are only significant corrections from small l. In our universe the density power spectrum is not an exact power law but may be approximately so at small and large scales. It is probable than on scales $\ll 100h^{-1}$Mpc that $n \approx -1$ while at large scales $n \approx 1$. We see that eq (5.18) diverges as $n \to 1$. This logarithmic divergence is regulated by a cutoff at small scales as explained above.

One can argue that the asymptotic approximation of eqs (A6) and (B9) is a very good approximation when applied to our own universe. This follows from the fact that for deep galaxy catalogs it is the large scales which are relevant for the small l. At these large scales $n \approx 1$, which is where eq (5.18) is extremely accurate for all l. It is true that this asymptotic approximation may be off by a $\sim 30\%$ at $l = 2$ for extremely shallow surveys, but as we shall see below one needs a fairly deep survey to measure the shear.

Small-Angle Limit

The small-angle shear has been studied extensively elsewhere and provides a useful check on our results so far. The large-l limit of I_l in eq (A7) is appropriate for small angle correlation functions. Taking this limit we find that (5.9) becomes

$$C_l^{\oplus}(r,r') \approx 18\pi^3 l \left(\frac{H_0}{a}\right)^4 \int_{\max(\frac{1}{r},\frac{1}{r'})}^{\infty} \frac{dk}{k^2} \left(1-\frac{l}{kr}\right)\left(1-\frac{l}{kr'}\right) P_\delta(k) \qquad l \gg 1. \tag{5.16}$$

Thus eq (4.37) becomes

$$\langle\gamma^2\rangle \approx \langle\kappa^2\rangle \approx \frac{1}{2\pi}\int_0^\infty dl\, l\, C_l^{\oplus}(r,r) = \frac{3\pi^2}{10}\left(\frac{H_0}{a}\right)^4 r^3 \int_0^\infty dk\, k\, P_\delta(k) \tag{5.17}$$

and using

$$\frac{H_0 r}{a} = 2\left(1-\frac{1}{\sqrt{1+z}}\right) \tag{5.18}$$

we finds that the rms shear at the redshift z is

$$\sqrt{\langle\kappa^2\rangle} = \sqrt{\langle\gamma^2\rangle} = 2\pi\left(1-\frac{1}{\sqrt{1+z}}\right)^{\frac{3}{2}}\left[\frac{3}{5}\frac{H_0}{a}\int_0^\infty dk\, k\, P(k)\right]^{\frac{1}{2}} \tag{5.19}$$

which agrees with eq (83) of Blandford *et al.* (1991) and eq (2.3.6) of Kaiser (1992). Note that the polarization, p, used in these papers is twice the shear, γ, used here. Furthermore Blandford *et al.* (1991) uses units where $H_0/a = 1$ while Kaiser (1992) uses units where $\frac{1}{2}H_0/a = 1$. Finally note that $P(k)$ in Kaiser (1992) is defined to be a factor $(2\pi)^3$ larger than that used here, while Blandford *et al.* (1991) use the same Fourier convention as here.

Distance-Limited Sample at Small Angles

Now let us consider the average shear in a spatially uniform sample going to a maximum distance $r_{\max}$, i.e. use the visibility function of eq (4.42). In the small angle limit we obtain

$$\overline{C_l^{\oplus}} \approx 18\pi^3 l \left(\frac{H_0}{a}\right)^4 \int_{\frac{1}{r_{\max}}}^\infty \frac{dk}{k^2}\left(1+\frac{l^3}{2(kr_{\max})^3}-\frac{3l}{2kr_{\max}}\right)^2 P_\delta(k) \tag{5.20}$$

and thus

$$\begin{aligned}\langle\overline{\gamma}^2\rangle \approx \langle\overline{\kappa}^2\rangle \approx \frac{1}{2\pi}\int_0^\infty dl\, l\, \overline{C_l^{\oplus}} &= \frac{17\pi^2}{140}\left(\frac{H_0}{a}\right)^4 {r_{\max}}^3 \int_0^\infty dk\, k\, P_\delta(k) \\ &= \frac{34\pi^2}{35}\left(1-\frac{1}{\sqrt{1+z_{\max}}}\right)^3 \frac{H_0}{a}\int_0^\infty dk\, k\, P_\delta(k)\end{aligned} \tag{5.21}$$

Comparing (5.21) to (5.17) we see that the average shear in a distance limited sample is roughly 0.64... times the shear at the edge of the sample.

Power Law Power Spectra for a Distance-Limited Sample

Now let us also specify the power spectrum, choosing a power-law overdensity correlation function

$$\xi(r) \equiv \langle\delta(\mathbf{x})\delta(\mathbf{x}')\rangle = \left(\frac{r_0}{r}\right)^{3+n} \qquad r = |\mathbf{x}-\mathbf{x}'| \tag{5.22}$$

which is equivalent to the power-law power spectrum

$$P_\delta(k) = \frac{r_0^{3+n}\Gamma(-\frac{n}{2})}{2^{3+n}\pi\sqrt{\pi}\Gamma(\frac{3+n}{2})}\, k^n \qquad -3 < n < 0. \tag{5.23}$$

Substituting this into (5.20) we obtain

$$l^2\overline{C_l^{\oplus}} \approx 324\pi\sqrt{\pi}\,(11-3n)\,(6-n)\,\frac{1}{l}\,\frac{\Gamma(-\frac{n}{2})\Gamma(1-n)}{\Gamma(\frac{3+n}{2})\Gamma(8-n)}\left(\frac{H_0 r_{\max}}{a}\right)^4\left(\frac{r_0 l}{2r_{\max}}\right)^{3+n} \qquad -3 < n < 0. \tag{5.24}$$

which is equivalent to 2nd expression in (5.18). The reason for the divergence at $n = 0$ is because the correlation length, r_0, is ill-defined for $n \geq 0$. Apart from this n-dependent divergence of the correlation length the l-dependence is correct for $n < 1$. For power law spectra the shear two-point correlation is given by

$$C_{\bar{\kappa}}(\vartheta) \approx \frac{81\sqrt{\pi}}{2}(11-3n)(6-n)\frac{\Gamma(1-n)}{\Gamma(8-n)}\frac{\Gamma(\frac{2+n}{2})}{\Gamma(\frac{3+n}{2})}\left(\frac{H_0 r_0}{a}\right)^{3+n}\left(\frac{H_0 r_{\max}}{a}\right)^{1-n}\frac{1}{\vartheta^{2+n}}$$
$$C_{\bar{\gamma}}(\vartheta,\varphi,\varphi') \approx C_{\bar{\kappa}}(\vartheta)\left(\cos 2(\varphi-\varphi') + \frac{(2+n)(4+n)}{n(n-2)}\cos 2(\varphi+\varphi')\right) \qquad -2 < n < 0. \quad (5.25)$$

The correlation functions diverge for $n < -2$ due to an infrared divergence. The integrals which give these correlation functions are formally convergent at large l for any n, however for $n > -1$ the contribution to the integral is dominated by the behaviour of the integrand at $l \gg 1/\vartheta$. Thus for large n the results obtained are sensitive to our assumption of exact power law behaviour over a broad range of scales.

One must be careful about evaluating these expressions for integer values of n. While it may appear that there is a singularity at $n = 0$, note that $C_{\bar{\kappa}}$ is zero at $n = 0$, and $C_{\bar{\gamma}}$ is smooth at $n = 0$. Note that these power-law spectra cause the correlation function be be singular at zero separation which leads to certain pathologies. For example $C_{\bar{\kappa}}$ is negative for all ϑ if $n > 0$ while the coefficient of $\cos 2(\varphi+\varphi')$ in $C_{\bar{\gamma}}$ has a positive divergence as $\vartheta \to 0$. If we were to regulate this divergence at small scales we would find that $C_{\bar{\kappa}}$ would be positive and finite at $\vartheta = 0$ while the coefficient of $\cos 2(\varphi+\varphi')$ in $C_{\bar{\gamma}}$ would go to zero.

While the power spectrum of mass fluctuations may indeed be a power law down to very small scales, we can only measure shear averaged over a finite region of the sky and this averaging decreases our sensitivity to the the divergent density fluctuations at large scales. On small scales, the convolution of the shear pattern with a Gaussian beam corresponds to multiplying the angular power spectrum by $\exp(-l^2\sigma^2)$ where σ is the "Gaussian width" of the beam, which is related to the FWHM by $\sigma_{\rm fwhm} = 2\sqrt{2\ln 2}\,\sigma$. For a Gaussian beam we obtain

$$\overline{C_{\bar{\kappa}}}(\vartheta) \approx 81\sqrt{\pi}(11-3n)(6-n)\frac{\Gamma(\frac{2+n}{2})\Gamma(-\frac{n}{2})\Gamma(1-n)}{\Gamma(\frac{3+n}{2})\Gamma(8-n)}\left(\frac{H_0 r_{\max}}{a}\right)^4\left(\frac{r_0}{2r_{\max}}\right)^{3+n}{}_1F_1\left(\frac{2+n}{2};1;-\frac{\vartheta^2}{4\sigma^2}\right)\frac{1}{\sigma^{2+n}} \quad (5.26)$$

where ${}_1F_1$ is a generalized hypergeometric function. Here we have used the notation $\overline{C_{\bar{\kappa}}}(\vartheta)$ to indicate that we are taking the correlation of the smoothed quantities. Simpler expressions can be found for the variance of zero-lag (i.e. $\vartheta = 0$) smoothed quantities :

$$\overline{C_{\bar{\kappa}}}(0) \approx 81\sqrt{\pi}(11-3n)(6-n)\,l^{1+n}\frac{\Gamma(\frac{2+n}{2})\Gamma(-\frac{n}{2})\Gamma(1-n)}{\Gamma(\frac{3+n}{2})\Gamma(8-n)}\left(\frac{H_0 r_{\max}}{a}\right)^4\left(\frac{r_0}{2r_{\max}}\right)^{3+n}\frac{1}{\sigma^{2+n}} \qquad -2 < n < 0.$$
$$\overline{C_{\bar{\gamma}}}(0,\varphi,\varphi') \approx \overline{C_{\bar{\kappa}}}(0)\cos 2(\varphi-\varphi') \quad (5.27)$$

6. Accuracy of Shear Measurements

When the shear is weak, i.e. when $\gamma \ll 1$, the way one goes about measuring shear is by looking for alignments in the apparent orientation of background galaxies. The implicit assumption is that there is no significant intrinsic alignment of galaxy ellipticities and any apparent alignment must be due to a coherent shear in the image. As discussed above this is not liable to be exactly true but is liable to be a excellent approximation. One can measure the apparent shape of galaxy, g, using the ellipticity tensor (Kaiser 1992) which is

$$e^g_{ab} = \frac{Q^g\,Q^g_{ab} - Q^g_a Q^g_b}{Q^g\,Q^g_{cc} - Q^g_c Q^g_c} - \frac{1}{2}\delta_{ab} = \frac{1}{2}e^g\begin{pmatrix}\cos 2\chi^g & \sin 2\chi^g \\ \sin 2\chi^g & -\cos 2\chi^g\end{pmatrix} \quad (6.1)$$

where Q^g, Q^g_b, Q^g_{ab} give the 0th, 1st, and 2nd moments of the galaxy brightness distribution on the sky. Here χ^g is position angle of the galaxy and $e^g \in [0,1]$ it's the ellipticity. If the true galaxy position angles are randomly oriented then the expected ellipticity is

$$\langle e^g_{ab}\rangle_g = (1 - \frac{1}{2}\overline{e^2})\,\gamma_{ab} \quad (6.2)$$

in the weak lensing approximation. Here $\langle\cdots\rangle_g$ indicates an ensemble average over galaxy orientations, and $\overline{e^2}$ gives the mean square ellipticity. Given the range of possible ellipticities the proportionality constant between ellipticity and shear varies by only a factor of 2 between perfectly circular galaxies, $e^g = 0$ and highly elongated galaxies, $e^g = 1$. The variation from the expected value is

$$\langle (e^g_{ab} - \langle e^g_{ab}\rangle_g)(e^{g'}_{cd} - \langle e^{g'}_{cd}\rangle_g)\rangle_g = \frac{1}{4}\overline{e^2}\delta_{gg'}(g_{ac}g_{bd} + \epsilon_{ad}\epsilon_{bc}) \tag{6.3}$$

where again g_{ac} is the metric on the sphere of the sky and ϵ_{ab} the Levi-Civita symbol. For perfectly circular galaxies, $e^g = 0$, the apparent position angle and shape gives the shear precisely, while for non-circular galaxies there is considerable variance. Typical intrinsic galaxy shapes have $\overline{e^2} \sim (0.3)^2$. Note that if one makes *random* measurement errors in the shapes of galaxies then one should add this in quadrature to the deviation from the expected value in eq (6.3). Given the fairly large intrinsic error due to galaxy non-circularness one would have to make rather large measurements errors to significantly increase ones uncertainty in the determination of the shear. Roughly speaking one needs $N \sim \overline{e^2}/[8(1 - \frac{1}{2}\overline{e^2})^2\gamma^2]$ objects to obtain a determination of the mean shear in a patch of the sky with S/N$\sim$ 1 if one has perfect measurements. Since typically one is looking for $\gamma \sim 0.01$ one needs significantly more than 100 perfectly measured galaxies or even more when one includes measurement errors. Of course the main problem in practice will be non-random measurement errors, i.e. errors in galaxy shapes which are correlated between different galaxies.

Below we will consider estimating the shear from a uniform all-sky survey of galaxies. We will allow for an arbitrary weighting of different galaxy types, given by a parameter w_g for each galaxy. This weighting might depend on the apparent shape (not orientation!) of the galaxies, the colors, or the apparent magnitude. Given this weighting there are a variety of different definitions of the number of galaxies in one survey, in particular one may define it with different powers of w_g, i.e.

$$N_{gn} = \frac{\left\langle \sum_g w_g^n \right\rangle_g}{4\pi} = \left\langle \sum_g w_g^n\, \delta^{(2)}(\hat{\mathbf{n}} - \hat{\mathbf{n}}_g) \right\rangle_g \tag{6.4}$$

where δ-functions are normalized such that

$$\int d^2\hat{\mathbf{n}}\, \delta^{(2)}(\hat{\mathbf{n}} - \hat{\mathbf{n}}_g) = 1. \tag{6.5}$$

and $\langle\cdots\rangle_g$ indicates an ensemble average over galaxy positions and orientations, but not over realizations of the shear distribution. This is only possible because we will be assuming that the galaxy distribution and shear distribution are independent. We do not expect this to be exactly correct, however it is probably a fairly good approximation since the galaxies which sheared are so far from the galaxies associated with the mass-distribution which is doing the shearing, that the correlations are fairly weak.

An estimator of the radially weighted shear is given by

$$\hat{\bar{\gamma}}_{ab}(\hat{\mathbf{n}}) = \frac{\sum_g w_g e^g_{ab}\delta^{(2)}(\hat{\mathbf{n}} - \hat{\mathbf{n}}_g)}{N_{g1}\left(1 - \frac{1}{2}\overline{e^2}\right)}. \tag{6.6}$$

One should, of course, not take the δ-functions as meaning the shear in concentrated in small patches of the sky, rather one should average this estimator over an angular patch large enough to contain many galaxies, and thereby obtain an estimator of the angle-averaged shear. Using the weak lensing formula, (6.2), we find that

$$\langle\hat{\bar{\gamma}}_{ab}(\hat{\mathbf{n}})\rangle_g = \langle\gamma_{ab}(r_g,\hat{\mathbf{n}})\rangle_g \frac{\left\langle \sum_g w_g\, \delta^{(2)}(\hat{\mathbf{n}} - \hat{\mathbf{n}}_g)\right\rangle_g}{N_{g1}} = \int_0^\infty dr V(r)\,\gamma_{ab}(r,\hat{\mathbf{n}}) = \bar{\gamma}_{ab}(\hat{\mathbf{n}}) \tag{6.7}$$

where we have defined the visibility function, $V(r)$:

$$V(r) = \frac{\left\langle \sum_g w_g \delta(r - r_g)\right\rangle_g}{4\pi N_{g1}}. \tag{6.8}$$

Here we have assumed isotropy and homogeneity on the sky, so that the radial and angular distribution of galaxies factorize. This shows that $\widehat{\bar{\gamma}}_{ab}(\hat{\mathbf{n}})$ is an unbiased estimator of $\bar{\gamma}_{ab}(\hat{\mathbf{n}})$. Of course one needs to know the distribution of galaxies in ones sample to determine $V(r)$ and thus to know what $\widehat{\bar{\gamma}}_{ab}(\hat{\mathbf{n}})$ is an unbiased estimator for. In the weak lensing limit we may use eq (6.3) to determine the mean square error in this estimator, which is

$$\left\langle \left(\widehat{\bar{\gamma}}_{ab}(r,\hat{\mathbf{n}}) - \bar{\gamma}_{ab}(r,\hat{\mathbf{n}})\right)\left(\widehat{\bar{\gamma}}_{cd}(r',\hat{\mathbf{n}}') - \bar{\gamma}_{cd}(r',\hat{\mathbf{n}}')\right)\right\rangle_{\mathbf{g}} = \frac{N_{\mathbf{g}2}}{4{N_{\mathbf{g}1}}^2}\,\frac{\overline{e^2}}{\left(1-\frac{1}{2}\overline{e^2}\right)^2}\left(g_{ac}g_{bd}+\epsilon_{ac}\epsilon_{bd}\right)\delta^{(2)}(\hat{\mathbf{n}}-\hat{\mathbf{n}}'). \tag{6.9}$$

Comparing this correlation function with $C_{\bar{\gamma}}$ of §4 we find the correlation function of the error in the estimator of eq (6.6):

$$C^{\mathbf{sn}}_{\bar{\gamma}}(\vartheta,\varphi,\varphi') = \frac{N_{\mathbf{g}2}}{4{N_{\mathbf{g}1}}^2}\,\frac{\overline{e^2}}{\left(1-\frac{1}{2}\overline{e^2}\right)^2}\cos 2(\varphi-\varphi')\lim_{\epsilon\to 0}\delta(1-\epsilon-\cos\vartheta) \tag{6.10}$$

where the superscript "sn" refers to the ***shot noise*** from the finite number of galaxies. We may also compute the power spectrum for the shot noise by substituting $C^{\mathbf{sn}}_{\bar{\gamma}}$ into (4.31):

$$C_l^{\oplus\mathbf{sn}} = C_l^{\otimes\mathbf{sn}} = \frac{\pi}{4}\,\frac{l(l+1)}{(l+2)(l-1)}\,\frac{N_{\mathbf{g}2}}{{N_{\mathbf{g}1}}^2}\,\frac{\overline{e^2}}{\left(1-\frac{1}{2}\overline{e^2}\right)^2}. \tag{6.11}$$

We see that the shot noise contributes equally to the scalar and pseudo-scalar part of the error. The shot noise is white noise, i.e. on small scales ($l \gg 1$) both $C_l^{\oplus\mathbf{sn}}$ and $C_l^{\otimes\mathbf{sn}}$ become l-independent. Substituting (6.11) into (4.27) we may compute the mean square error in the shear for all modes with $l < L$ is

$$\langle\overline{\gamma^{\mathbf{sn}}_{l\le L}}^2\rangle = \frac{N_{\mathbf{g}2}}{8{N_{\mathbf{g}1}}^2}\,\frac{\overline{e^2}}{\left(1-\frac{1}{2}\overline{e^2}\right)^2}\sum_{l=2}^{L}(2l+1) = \frac{N_{\mathbf{g}2}}{8{N_{\mathbf{g}1}}^2}\,\frac{\overline{e^2}}{\left(1-\frac{1}{2}\overline{e^2}\right)^2}(L+3)(L-1) \qquad L\ge 2. \tag{6.12}$$

At small angles the mean square shot-noise in a Gaussian beam is

$$\langle\overline{\gamma^{\mathbf{sn}}}^2\rangle \approx \frac{N_{\mathbf{g}2}}{8{N_{\mathbf{g}1}}^2}\,\frac{\overline{e^2}}{\left(1-\frac{1}{2}\overline{e^2}\right)^2}\int_0^\infty dl\,2l\,e^{-l^2\sigma^2} = \sqrt{\pi\ln 2}\,\frac{N_{\mathbf{g}2}}{{N_{\mathbf{g}1}}^2}\,\frac{\overline{e^2}}{\left(1-\frac{1}{2}\overline{e^2}\right)^2}\,\frac{1}{\sigma^2_{\mathbf{fwhm}}}. \tag{6.13}$$

where we have used $\sigma_{\mathbf{fwhm}} = 2\sqrt{2\ln 2}\,\sigma$.

Estimators for $C_l^\oplus$ and $C_l^\oplus$

A sum of unbiased estimators of some quantities is itself an unbiased estimator of the sum. Thus combining (6.6) with (4.12) we can construct unbiased estimators of the spherical harmonic amplitudes which describe the shear field

$$\begin{aligned}
\widehat{\phi^{\oplus}_{(l,m)}}^{\mathbf{g}} &= -2\,\frac{(l-2)!}{(l+2)!}\,\frac{1}{N_{\mathbf{g}1}\left(1-\frac{1}{2}\overline{e^2}\right)}\sum_g w_g\,Y^*_{(l,m)}{}^{:ab}(\hat{\mathbf{n}}_g)\,e^g_{ab}\\
\widehat{\phi^{\otimes}_{(l,m)}}^{\mathbf{g}} &= -2\,\frac{(l-2)!}{(l+2)!}\,\frac{1}{N_{\mathbf{g}1}\left(1-\frac{1}{2}\overline{e^2}\right)}\sum_g w_g\,Y^*_{(l,m)}{}^{:ac}(\hat{\mathbf{n}}_g)\,e^g_{ad}\,\epsilon_c{}^d
\end{aligned}. \tag{6.14}$$

The superscript g emphasizes that these are estimators derived from a galaxy sample. One can construct estimators of the $C_l^\oplus$ and $C_l^\otimes$ using eq (4.13)

$$\widehat{C_l^{\oplus}}^{\mathbf{g}} = -C_l^{\oplus\mathbf{sn}} + \frac{l^2(l+1)^2}{4(2l+1)}\sum_{m=-l}^{l}\left|\widehat{\phi^{\oplus}_{(l,m)}}^{\mathbf{g}}\right|^2 \qquad \widehat{C_l^{\otimes}}^{\mathbf{g}} = -C_l^{\otimes\mathbf{sn}} + \frac{l^2(l+1)^2}{4(2l+1)}\sum_{m=-l}^{l}\left|\widehat{\phi^{\otimes}_{(l,m)}}^{\mathbf{g}}\right|^2. \tag{6.15}$$

These are unbiased because the shot noise has been subtracted and differ from those in eq (4.13) since those were estimators derived from perfect knowledge of the shear pattern on the sky, while these include additional uncertainties

due to finite galaxy sampling. Of course real surveys will probably never cover the entire sky and other estimators must constructed to deal with finite sky coverage.

The mean square deviation of $\widehat{C_l^{\oplus}}^{\mathcal{S}}$ and $\widehat{C_l^{\otimes}}^{\mathcal{S}}$ from $C_l^{\oplus}$ and $C_l^{\otimes}$ will depend on the 4-point correlation function of the shear as well as the clustering properties of the galaxies. We will not go into such detail here, instead we assume Gaussian statistics, i.e. set the reduced 4-point function to zero, and assume Poisson sampling of the shear field. These approximations are liable to be good ones for deep samples on large angular scales. In any case, better estimates of the uncertainties should be computed. With these assumptions we find

$$\begin{aligned}
\left\langle \left(\widehat{C_l^{\oplus}}^{\mathcal{S}} - C_l^{\oplus}\right)\left(\widehat{C_{l'}^{\oplus}}^{\mathcal{S}} - C_{l'}^{\oplus}\right)\right\rangle &= \delta_{ll'}\,\frac{2}{2l+1}\,(C_l^{\oplus 2} + C_l^{\oplus \mathrm{sn}^2}) \\
\left\langle \left(\widehat{C_l^{\otimes}}^{\mathcal{S}} - C_l^{\otimes}\right)\left(\widehat{C_{l'}^{\otimes}}^{\mathcal{S}} - C_{l'}^{\otimes}\right)\right\rangle &= \delta_{ll'}\,\frac{2}{2l+1}\,(C_l^{\otimes 2} + C_l^{\otimes \mathrm{sn}^2}) \\
\left\langle \left(\widehat{C_l^{\oplus}}^{\mathcal{S}} - C_l^{\oplus}\right)\left(\widehat{C_{l'}^{\otimes}}^{\mathcal{S}} - C_{l'}^{\otimes}\right)\right\rangle &= 0
\end{aligned} \tag{6.16}$$

so that the 1-σ fractional uncertainty is

$$\frac{\Delta C_l^{\oplus}}{C_l^{\oplus}} = \sqrt{\frac{2}{2l+1}\left(1 + \frac{C_l^{\oplus \mathrm{sn}^2}}{C_l^{\oplus 2}}\right)} \qquad \frac{\Delta C_l^{\otimes}}{C_l^{\otimes}} = \sqrt{\frac{2}{2l+1}\left(1 + \frac{C_l^{\otimes \mathrm{sn}^2}}{C_l^{\otimes 2}}\right)}. \tag{6.17}$$

The 1st term in the radical represents cosmic variance which is more dominant for small l, while the second is uncertainty due to shot noise which is more dominant at large l. With the above estimate of the error one can define a total signal-to-noise:

$$\begin{aligned}
\left(\frac{\mathrm{S}^{\oplus}}{\mathrm{N}^{\oplus}}\right)^2 &= \sum_l \left(\frac{C_l^{\oplus}}{\Delta C_l^{\oplus}}\right)^2 = \sum_l \frac{2l+1}{2}\,\frac{C_l^{\oplus 2}}{C_l^{\oplus 2} + C_l^{\oplus \mathrm{sn}^2}} \\
\left(\frac{\mathrm{S}^{\otimes}}{\mathrm{N}^{\otimes}}\right)^2 &= \sum_l \left(\frac{C_l^{\otimes}}{\Delta C_l^{\otimes}}\right)^2 = \sum_l \frac{2l+1}{2}\,\frac{C_l^{\otimes 2}}{C_l^{\otimes 2} + C_l^{\otimes \mathrm{sn}^2}}
\end{aligned} \tag{6.18}$$

which should be greater than unity in the range of l of interest if one is capable of detecting a significant shear. Note that these signal-to-noise ratios include cosmic variance.

7. A Realistic Example

Now let us estimate the angular power spectrum of the shear we might expect to find in our own universe. Clearly there are large uncertainties in the distribution in mass in our universe so we cannot predict precisely what one will see. In fact the utility of weak lensing is to measure the mass distribution. Here we give a rather simple empirically based model, which is meant to be optimistic about the size of the shear which one might find. We are also not very realistic about the data one is liable to collect. For example we assume an all-sky volume limited sample of galaxies, while one is really liable to obtain a partial-sky magnitude-limited sample. More detailed studies clearly should be done.

On small scales the correlation function of optically selected galaxies appears to be approximately a power law (Peebles 1980) as was assumed for the mass in eq (5.22-27). Taking parameters. $r_0 = 5\,h^{-1}$Mpc and $n = -1.2$, which are close to the values obtained observationally (Humit *et al.* 1996) we find

$$\begin{aligned}
C_{\overline{\kappa}}(\vartheta) &\approx (0.0180)^2\left(1 - \frac{1}{\sqrt{1+z_{\mathrm{max}}}}\right)^{2.2}\left(\frac{1^\circ}{\vartheta}\right)^{0.8} \approx (0.0084)^2 {z_{\mathrm{max}}}^{2.2}\left(\frac{1^\circ}{\vartheta}\right)^{0.8} \\
C_{\overline{\gamma}}(\vartheta,\varphi,\varphi') &\approx C_{\overline{\kappa}}(\vartheta)\;(\cos 2(\varphi-\varphi') + 0.5833\cos 2(\varphi+\varphi')) \\
\overline{C_{\overline{\kappa}}}(0) &\approx (0.0235)^2\left(1 - \frac{1}{\sqrt{1+z_{\mathrm{max}}}}\right)^{2.2}\left(\frac{1^\circ}{\sigma_{\mathrm{fwhm}}}\right)^{0.8} \approx (0.0110)^2 {z_{\mathrm{max}}}^{2.2}\left(\frac{1^\circ}{\sigma_{\mathrm{fwhm}}}\right)^{0.8}. \\
\overline{C_{\overline{\gamma}}}(0,\varphi,\varphi') &\approx \overline{C_{\overline{\kappa}}}(0)\cos 2(\varphi-\varphi') \\
l^2\overline{C_l^{\oplus}} &\approx \left(\frac{l}{1.8\times 10^5}\right)^{0.8}\left(1 - \frac{1}{\sqrt{1+z_{\mathrm{max}}}}\right)^{2.2} \approx \left(\frac{l}{1.2\times 10^6}\right)^{0.8} {z_{\mathrm{max}}}^{2.2}
\end{aligned} \tag{7.1}$$

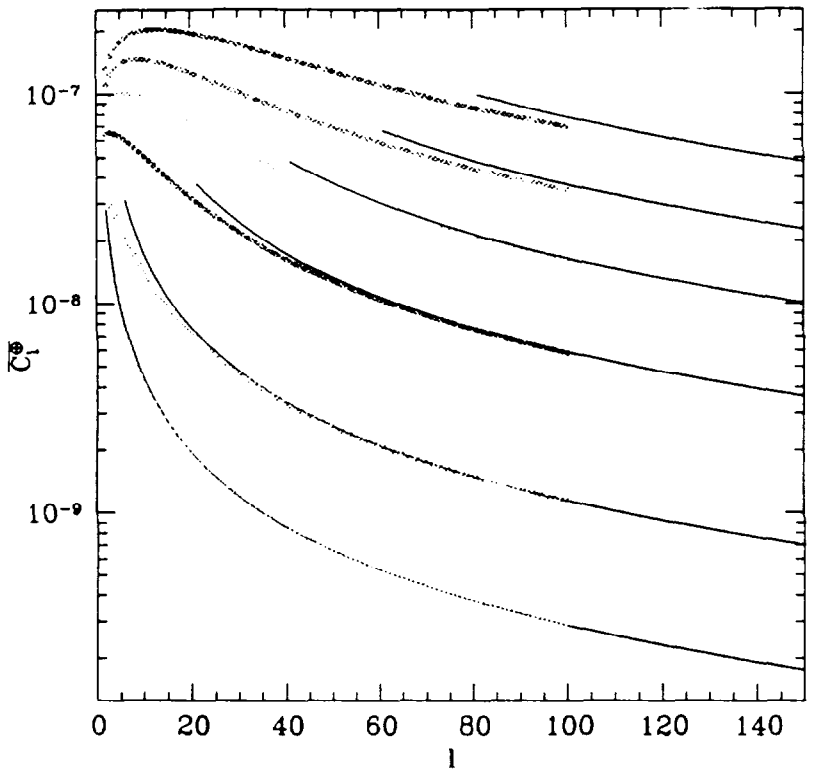

Figure 4: Plotted as a function of l, for a volume limited survey in an Einstein-deSitter universe is $\overline{C_l^{\oplus}}$ obtained for an unbiased COBE-normalised model of adiabatic density fluctuations given by eq (7.3). The yellow, green blue, cyan, magenta, and red points are for a limiting survey redshift of z_{max} =0.1, 0.2, 0.5, 1, 2, and 5 respectively. The corresponding solid lines give the $\overline{C_l^{\oplus}}$ for the same limiting redshift but using the asymptotic approximation and assuming the the small scale power law index $n = -1.2$ on all scales. The deviation of the solid lines from the points is primarily due to the turnover in the spectrum at large scales, which greater for deeper surveys and smaller l because these probe larger comoving scales. The large l behaviour is described by eq (7.2), i.e. $C_l^{\oplus} \propto l^{-1.2} z_{max}{}^{2.2}$, while for deep enough surveys, $z_{max} \gtrsim 1$, eq (5.16) describes the behaviour, i.e. $C_l \propto l$ with only a weak depth dependence.

where expressions proportional to $z_{max}{}^{2.2}$ are appropriate for $z_{max} \ll 1$. This power law behaviour certainly does not persist to very large scales and it is generally believed that the spectrum turns over to something close to a Harrison-Zel'dovich spectrum ($n = 1$) at large scales. As a model of the power spectrum of density inhomogeneities on both small and large scales we will use

$$P_\delta(k) = \frac{Ak}{(1+(kr_{HS})^2)^{1.1}} \qquad A = \frac{r_{HS}{}^{2.2} r_0^{1.8} \Gamma(0.6)}{2^{1.8}\pi\sqrt{\pi}\Gamma(0.9)}\,. \tag{7.2}$$

where we again use $r_0 = 5\,h^{-1}$Mpc and $n = -1.2$ and supplement it with $r_{HS} = 38.8h^{-1}$Mpc which matches the COBE normalization for adiabatic initial conditions.

In fig 4 is plotted $C_l^{\oplus}$ from this model for various survey depths, z_{max}, and compare this with the result we would obtain if we used the asymptotic approximation of eq (5.9) combined with pure power law spectrum of eqs (5.22-24) on all scales. This figure illustrates that the approximations used to derive eq (7.1) are accurate on all angular scales for shallow surveys, and on small angular scales power law model for deeper surveys. In fig 5 we plot the rms shear contributed by angular scales larger than a given scale, as a function of the minimal scale, again for various values of depth. On the largest angular scales one may only find a shear of $\sim 10^{-4}$. We will argue below that there will be no significant signal for $z_{max} \lesssim 0.1$ so we see that for interesting surveys one is looking for a shear $\gtrsim 3 \times 10^{-4}$. For such a level of shear one needs $\gtrsim 10^5$ galaxies with good shape information to detect it. One might need many more if the galaxy shapes have large statistical or systematic errors. Of course as one goes deeper one needs fewer galaxies. One critical issue is whether one is able to make absolute measurements of the shear. If one can then one is sensitive to all angular scale larger than the area one surveys. Absolute measurements are possible in principle as one can use

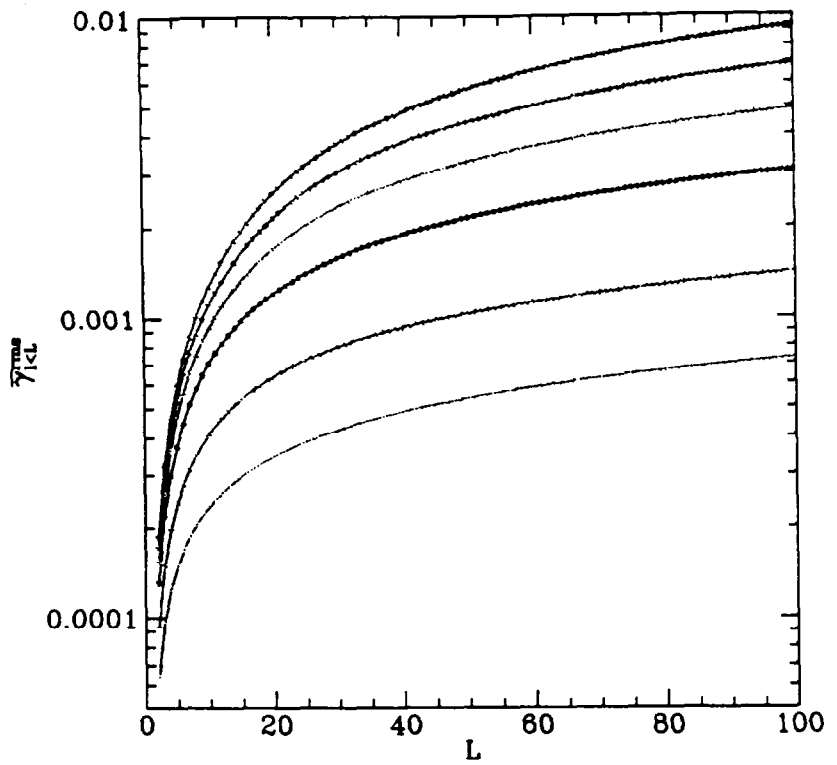

Figure 5: Plotted versus L is the rms shear contributed by modes with angular wavenumber $l < L$. As in fig 3 these are for the power spectrum model of eq (7.3) and the yellow, green blue, cyan, magenta, and red points are for a limiting survey redshift of z_{max} =0.1, 0.2, 0.5, 1, 2, and 5 respectively. The the solid lines are to guide the eye. For $l \gg 1$ this also gives the rms expansion, κ, which is gives the source amplification.

stellar images to correct for instrumentally or atmospherically induced shear (Kaiser, Squires, and Broadhurst 1995). If for some reason one is limited to differential measurements of shear then for small survey areas one loses much of the signal. Except for small l the $\gamma_{rms} \approx \kappa_{rms}$ so that fig 5 also gives the image amplification. Broadhurst, Taylor, and Peacock (1995) have proposed a methodology to statistically measure amplification due to gravitational lensing and applied it in Broadhurst (1995).

Some will argue that we the simple mass model used here is probably an overestimate of the magnitude of the shear. The author considers it an optimistic estimate, but not wildly so. For non-adiabatic perturbations the large scale density inhomogeneities are less than assumed here. Furthermore it has long been argued that the mass inhomogeneities on the $8\,h^{-1}$Mpc scale are smaller than the galaxy inhomogeneities (e.g. Henry & Arnaud 1991, White, Efstathiou, and Frenk 1993), so that we may also be overestimating the lensing on small scales as well. Furthermore the model power spectrum used here clearly has some contribution from non-linear clustering, which is not quite consistent with the linear evolution of density perturbations we have assumed in §5. Corrections for the non-linear evolution of the power spectrum will be important for deep samples, $z \gtrsim 0.5$, on small angular scales. If galaxies are biased tracers of the mass distribution or if the universe is not flat then, with fixed $\delta\rho/\rho$, the lensing shear at small redshifts scales proportionate to Ω_0/b, where b is the bias factor. The reader may wish to apply this correction using his favorite values, which for many probably means reducing the predicted shear by at most a factor of 2 on small angular scales.

Here is considered a volume limited survey, up to redshift z_{max}, and assume no evolution in the number density, which is given by $\Phi^\star_g$, and use uniform weighting of all galaxies within the survey volume, i.e. $w_g = 1$. Using eq (6.8) we find

$$N_g \equiv N_{g1} = N_{g2} = \Phi^\star_g \left[\frac{2c}{H_0}\left(1 - \frac{1}{\sqrt{1+z_{max}}}\right)\right]^3 = 2.6\times 10^9 \left(1 - \frac{1}{\sqrt{1+z}}\right)^3 \qquad (7.3)$$

where we have taken $\Phi^\star_g = 0.012\,h^3/\mathrm{Mpc}^3$ which is the value of this parameter in the Schechter which describes

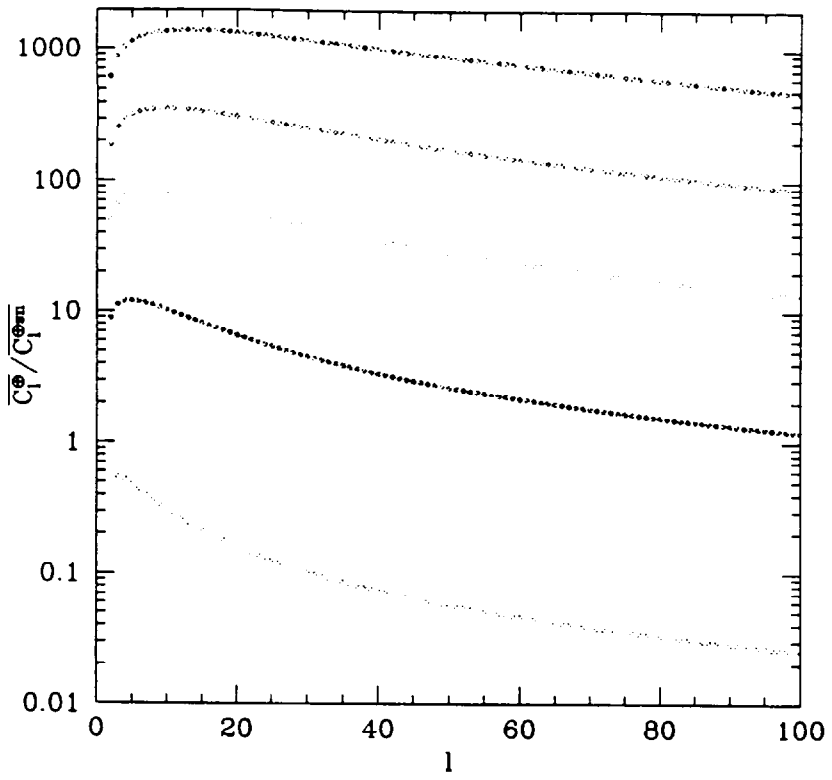

Figure 6: Plotted versus l is the ratio of the shear power $\overline{C_l^{\oplus}}$ to that induced by finite galaxy sampling in a volume limited survey with with rms ellipticity 0.3 and galaxy density $0.012(h/\mathrm{Mpc})^3$. As in figs 3&4 these are for the power spectrum model of eq (7.3) and the yellow, green blue, cyan, magenta, and red points are for a limiting survey redshift of z_{max} =0.1, 0.2, 0.5, 1, 2, and 5 respectively.

observed galaxies (Loveday *et al.* 1992). Taking $\overline{e^2} \approx (0.3)^2$ we find

$$C_l^{\oplus sn} = C_l^{\otimes sn} = 3.0 \times 10^{-11} \frac{l(l+1)}{(l+2)(l-1)} \left(1 - \frac{1}{\sqrt{1+z}}\right)^{-3} \tag{7.4}$$

so that

$$\sqrt{\langle \overline{\gamma_{l\le L}^{sn}}^2 \rangle} = 6.9 \times 10^{-6} \sqrt{(L+3)(L-1)} \left(1 - \frac{1}{\sqrt{1+z}}\right)^{-\frac{3}{2}}. \tag{7.5}$$

The minimum shot noise occurs when one includes only the quadrupole and at maximum depth, i.e. $L = 2$ and $z = \infty$, which yields $\sqrt{\langle \overline{\gamma_{l=2}^{sn}}^2 \rangle} = 4.8 \times 10^{-6}$. This is extremely small, much smaller than the expected signal on these scales. While going to very large redshifts may never be feasible, going to $z = 1$, which seems feasible, brings this up to 3.0×10^{-5}. Measurements to date have detected shear at the level of a few percent. We see that by doing very large area and very deep surveys one may in principle measure the shear down to a level up to 1000 times smaller. One may run into uncorrectable systematic errors long before one reaches this level, however it is certainly worth the effort get as close to the shot noise limit as possible.

Comparison of Shot Noise With Signal

It is interesting to compare the shot-noise "signal" with that which one might expect to obtain from density fluctuations. Of course density fluctuations produce no pseudo-scalar shear, so we need only compare the scalar

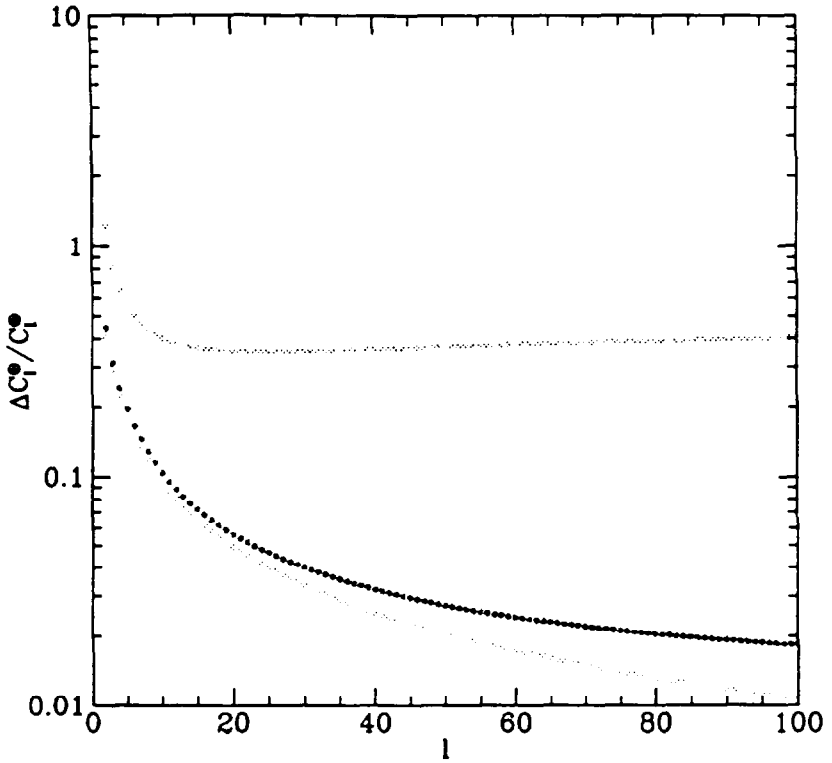

Figure 7: Plotted versus l is an estimate of the fractional uncertainty (1-σ) in the measurement of $C_l^{\oplus}$ from a volume limited sample with rms ellipticity 0.3 and galaxy density $0.012(h/\mathrm{Mpc})^3$. This uncertainty, taken from eq (6.17), includes the effects of finite galaxy sampling and cosmic variance. As in figs 3 – 5 these are for the power spectrum model of eq (7.?). The yellow, green blue, and cyan points are for a limiting survey redshift of z_{max} =0.1, 0.2, 0.5, and 1. The smallest fractional uncertainty, for z_{max} = 1 is dominated by cosmic variance for the l's plotted. One cannot significantly reduce this by going to a greater depth. Less deep surveys are significantly degraded by finite galaxy numbers. A sample with z_{max} = 0.1 survey would yield a marginally significant result by combining all l-modes. One would not obtain a significant signal for z_{max} significantly less than 0.1.

component of the shear. Comparing eq (5.20) with eq (6.11) we find

$$\frac{\overline{C_l^{\oplus}}}{C_l^{\oplus sn}} = 144\pi \frac{(l+2)!}{(l-2)!} \frac{{N_{g1}}^2}{N_{g2}} \frac{\left(1-\frac{1}{2}\overline{e^2}\right)^2}{\overline{e^2}} \left(\frac{H_0}{a}\right)^4 \int_0^{\infty} \frac{dk}{k^2} |\overline{I_l(k)}|^2 P_\delta(k)$$
$$\longrightarrow_{l\gg 1} \frac{9}{2}\pi l^3 N_g \frac{\left(1-\frac{1}{2}\overline{e^2}\right)^2}{\overline{e^2}} \left(\frac{H_0}{a}\right)^4 \int_{l/r_{max}}^{\infty} \frac{dk}{k^2} \left(\frac{2}{l} + \frac{l^2}{(kr_{max})^3} - \frac{3}{kr_{max}}\right)^2 P_\delta(k) \tag{7.6}$$

where we have used eq (A7) for the small angle limit and eq (5.20) for the volume-limited survey. This ratio is plotted in fig 6 and we see that for our model this signal-to-noise exceeds unity in each angular wavenumber, l, for all-sky surveys with $z_{max} \gtrsim 0.2$. Of course, as one decreases the sky coverage this signal-to-noise goes down.

If fig 7 is plotted the fractional uncertainty in a measurement of $C_l^{\oplus}$ according to eq (6.18). This includes cosmic variance, i.e. the additional uncertainty in one's determination of the global average of quantities due to the sample variance associated from looking at the universe from one vantage point. From this fractional uncertainty one can compute the total signal-to-noise defined in eq (6.18). This signal-to-noise includes from cosmic variance, unlike the ratio of eq (7.6). It is perhaps most interesting to consider the $\frac{S^{\oplus}}{N^{\oplus}}$ where it is close to unity. This leads us to consider shallow all-sky surveys where the contribution to $\frac{S^{\oplus}}{N^{\oplus}}$ from each individual l is much less than unity. From fig 7 it is clear that $\frac{S^{\oplus}}{N^{\oplus}}$ should grow greater than unity for $0.1 \lesssim z_{max} < 0.2$. For this range of z_{max} it is clear from fig 4 that the power law approximations of eqs (7.1) are a good approximation for nearly all l. We see from fig 7 that cosmic variance gives a negligible contribution to $\Delta C_l^{\oplus}$ for all l with z_{max} this small. Furthermore it is clear that one can

approximate the sum of eq (6.18) with an integral and take the large-l limit of both $C_l^{\oplus}$ and $C_l^{\oplus sn}$. Combining all of these approximations we find that for an all-sky survey

$$\left(\frac{S^{\oplus}}{N^{\oplus}}\right)^2 \approx \int_2^{\infty} dl\, l\, \frac{C_l^{\oplus 2}}{C_l^{\oplus sn\,2}} \approx \left(\frac{z_{max}}{0.11}\right)^{10.4} \qquad z_{max} \lesssim 0.2. \tag{7.7}$$

The l-integral converges relatively slowly, so that half the contribution comes from $l \leq 10$ and half from $l > 10$. The depth at which this signal-to-noise exceeds unity is not strongly dependent on the assumed amplitude of inhomogeneities, for example if we were decrease the density inhomogeneities by a factor of 2 this would change value of z_{max} at which $\frac{S^{\oplus}}{N^{\oplus}}$ equals unity from 0.11 to 0.15. For fractional sky coverage, f_{sky}, we expect $\frac{S^{\oplus}}{N^{\oplus}} \propto f_{sky}^{1/2}$, although this depends in detail on the geometry of the region surveyed. If one makes absolute shear measurements on a small patch of the sky then one has limited ability to determine on which angular scale the shear is generated. The extremely strong dependence on z_{max} exhibited by eq (7.7) breaks down for $z_{max} \gtrsim 0.2$ as one starts to sample the turnover in the density power spectrum.

8. Summary and Future Development

In this paper was presented a formalism of tensor spherical harmonics on the sphere which may be used to describe a weak lensing shear pattern over the entire celestial sphere. Many useful formula are presented in this paper but little in the form of derivations. A more complete exposition can be found on the world wide web at http://www-astro-theory.fnal.gov/Personal/stebbins/WeakLens/ . It was shown that in the all-sky shear pattern may be decomposed into geometrically distinct components: scalar shear and pseudo-scalar shear. In the weak lensing limit only scalar shear is produced by density inhomogeneities, and this is liable to be the only significant component of the shear field. Pseudo-scalar shear may be produced by vector and tensor perturbations, although the amplitude is liable to be negligible. On small scales one may also get significant pseudo-scalar shear when the lensing becomes strong due to more than one mass concentration along the line-of-sight. Given that one expects negligible pseudo-scalar shear on the sky, it's primary use is liable to be as a gauge of measurement errors.

In §5 the formalism was applied specifically to density inhomogeneities in an Einstein-deSitter cosmology, and in §6 to the study the shot noise one will obtain when trying to measure the shear with a finite number of galaxies. In §7 we apply the formalism derived to a model of the density perturbations in our universe. We illustrate that there is, in principle, a significant signal for wide area galaxy surveys even if one does not have a very deep galaxy sample. For example an all-sky survey of galaxies with redshifts less than 0.2 should exhibit a very significant signal of shear from gravitational lensing if one could reduce systematic errors below the 5×10^{-4} level in shear. A concerted observational effort should be made to see just how small a shear can be reliably measured with present technology from the ground. It should be noted that shallow surveys do benefit from the fact that the galaxies subtend a significantly larger angle than in deep surveys and thus there is less of a problem with seeing a finite pixelization. Given the large signal-to-noise which is present it is clear that some day such shallow large area shear maps will be made, but one may have to wait for large space-based optical surveys of the sky to be made.

The estimates of the expected shear presented in this paper are rather crude in that they assumed a volume limited survey and did not properly take into account the evolution of nonlinear clustering. Furthermore the error estimates assumed Gaussian statistics. Shallow surveys even over large areas sample the nonlinear clustering regime which is non-Gaussian. Proper estimates of the accuracy with which one can measure the shear should include the proper sample variance for the non-Gaussian density field. Again further study is needed.

Both shear and the linear polarization of light are described by a traceless symmetric rank-2 tensor on the celestial sphere and most of the mathematic formulae presented here can equally well be applied to a description of the linear polarization light on the celestial sphere. Kamionkowski, Kosowsky, and Stebbins (1996) have applied the tensor harmonic decomposition to a description of the cosmic microwave background radiation (CMBR). Just as with shear, density inhomogeneities (i.e. scalar modes) cannot, in linear theory, produce pseudo-scalar linear polarization of light. However in contrast to shear, vector and tensor modes can produce polarization of amplitude comparable to that produced by density inhomogeneities. Thus one may interpret any pseudo-scalar component of linear polarization of the CMBR as a direct detection of vector and/or tensor modes. This is in contrast to CMBR anisotropy where one cannot distinguish anisotropy induced by scalar modes from that produced by vector or tensor.

Acknowledgements: The author would like to thank Josh Frieman, Donn MacMinn, Uros Seljak, and Nick Kaiser for useful conversations. Special thanks to Marc Kamionkowski who has looked over some of the formalism. This work was supported by the NASA grant NAG 5-2788.

Appendix: Calculating $I_l(x)$

In this paper we have introduced the function

$$\begin{aligned} I_l(x) &= \int_0^1 \frac{dy}{y}(1-y)\, j_l(xy) \\ &= \frac{\sqrt{\pi}}{2^{l+1}\Gamma(\frac{3}{2}+l)}\, x^l \left(\frac{1}{l}\, {}_1F_2(\frac{l}{2}; \frac{l+2}{2}, \frac{3}{2}+l; -\frac{x^2}{4}) - \frac{1}{(l+1)}\, {}_1F_2(\frac{l+1}{2}; \frac{l+3}{2}, \frac{3}{2}+l; -\frac{x^2}{4}) \right) \end{aligned} \tag{A1}$$

where ${}_1F_2$ is a generalized Hypergeometric function which can be written in terms of sines, cosines, and Sine integrals. Specific cases are

$$\begin{aligned} I_1(x) &= \frac{-2x + x\cos x + \sin x + x^2 \mathrm{Si}x}{2x^2} \\ I_2(x) &= \frac{1}{3} - \frac{x\cos x - \sin x + x^2 \mathrm{Si}x}{2x^3} \\ I_3(x) &= \frac{-16x^3 - 3x(10-x^2)\cos x + 3(10+x^2)\sin x + 3x^4 \mathrm{Si}x}{24x^4} \\ I_4(x) &= \frac{2}{15} - \frac{3x(14+x^2)\cos x - (42-11x^2)\sin x + 3x^4 \mathrm{Si}x}{8x^5} \end{aligned} \tag{A2}$$

where the sine integral function, Si, is

$$\mathrm{Si}(x) = \int_0^x \frac{dx}{x} \sin x. \tag{A3}$$

These expressions become increasingly more complicated for large l and can involve enormous cancelation between terms. While symbolic algebra program do provide a generalized Hypergeometric functions, they are generally noisy for large arguments. Luckily one can derive accurate methods of calculating $I_l(x)$ based on the asymptotic expansions of this function. Using the Taylor series expansion of the spherical Bessel function in the definition of I_l we find

$$I_l(x) = \sum_{n=0}^{\infty} \frac{(-1)^n\, x^{2n+l}}{2^n (2(l+n)+1)!!\, n!\, (2n+l)\,(2n+l+1)}. \tag{A4}$$

For large x it we can expand $I_l(x)$ in powers of $1/x$ yielding

$$I_l(x) = \frac{\sqrt{\pi}}{l} \left(\frac{1}{2} \frac{\Gamma(\frac{l+2}{2})}{\Gamma(\frac{l+3}{2})} - \frac{1}{x} \frac{\Gamma(\frac{l+1}{2})}{\Gamma(\frac{l}{2})} \right) + \mathcal{O}(\frac{1}{x^2}). \tag{A5}$$

Between the series of (A4) for $x \lesssim l$ and the series (A5) for $x \gtrsim l$ one can compute $I_l(x)$ accurately for all values of x as long as l is not too large. While these series involves significant cancelation for $x \sim l$ one can use symbolic algebra programs to exactly compute the series up to a given order for rational values of x and interpolate in between.

Asymptotic Approximation and Small-Angle Limit

For large l one finds that $I_l(x)$ is well approximated by just the asymptotic form of (A5) where this is positive, and where (A5) is negative $I_l(x)$ is negligibly small, i.e.

$$I_l(x) \approx \left(a_l - \frac{b_l}{x}\right) \mathcal{H}\left(x - \frac{b_l}{a_l}\right) \qquad a_l = \frac{\sqrt{\pi}}{2l} \frac{\Gamma(\frac{l+2}{2})}{\Gamma(\frac{l+3}{2})} \qquad b_l = \frac{\sqrt{\pi}}{l} \frac{\Gamma(\frac{l+1}{2})}{\Gamma(\frac{l}{2})} \tag{A6}$$

where $\mathcal{H}()$ is the Lorentz-Heaviside function which is unity for positive argument and zero otherwise. Taking the large l limit of the factorial ratios this becomes

$$I_l(x) \approx \sqrt{\frac{\pi}{2l}} \left(\frac{1}{l} - \frac{1}{x}\right) \mathcal{H}(x-l) \qquad l \gg 1. \tag{A7}$$

The the fractional error of (A7) goes to zero for large l and $x > l$ while the absolute error goes to zero for large l and $x < l$.

Volume Average: $\overline{I_l}$

In this paper we have considered the mean shear from uniform distance limited in an Einstein-deSitter cosmology where the gravitational potential is assumed to be constant. In this case one use $\overline{I_k}$ defined in eq (5.12) with the visibility function of eq (4.42) to compute the mean shear. The Taylor series of the resultant function is

$$\overline{I_l}(x_{\max}) = 3\sum_{n=0}^{\infty} \frac{(-1)^n\, {x_{\max}}^{2n+l}}{2^n\,(2(l+n)+1)!!\,n!\,(2n+l)(2n+l+1)\,(2n+l+3)} \qquad x_{\max} \equiv k r_{\max}. \tag{A8}$$

Note that by making $\overline{I_l}$ a function of $kr_{\max}$ rather than just k we are using a slightly different notation than in the body of the paper. One may defined an asymptotic approximation just as in eq (A6) which is

$$\overline{I_l}(x_{\max}) \approx \left(a_l - \frac{3}{2}\frac{b_l}{x_{\max}} + \frac{1}{2}\frac{b_l^3}{a_l^2 {x_{\max}}^3}\right) \mathcal{H}\left(x_{\max} - \frac{b_l}{a_l}\right) \tag{A9}$$

where a_l and b_l are defined just as in eq (A6). The large l limit of this function is

$$\overline{I_l}(x_{\max}) \approx \frac{1}{l}\sqrt{\frac{\pi}{2l}}\left(1 - \frac{3}{2}\frac{l}{x_{\max}} + \frac{1}{2}\frac{l^3}{{x_{\max}}^3}\right) \mathcal{H}(x_{\max} - l) \qquad l \gg 1. \tag{A10}$$

Numerically the function $\bar{I}_l$ as a function of $x_{\max}$ is not very different than the I_l as a function of x.

References

R. Blandford, A. Saust, T. Brainerd, and J. Villumsen, *The distortion of distant galaxy images by large-scale structure*, ***M.N.R.A.S.*** **251** (1991), 600-627.

H. Bonnett, Y. Mellier, and B. Fort, *First detection of a gravitational weak shear at the periphery of cl0024+1654*, *Astrophys. J., Lett.* **427** (1994), L83.

T. Broadhurst, *Gravitational convergence and cluster masses*, astro-ph9511150.

T. Broadhurst, A. Taylor, and J. Peacock, *Mapping cluster mass distributions via gravitational lensing of background galaxies*, *Astrophys. J.* **438** (1995), 49-61.

G. Fahlman, N. Kaiser, G. Squires, and D. Woods, *Dark matter in ms1224 for distortions of background galaxies.*, *Astrophys. J.* **437** (1994), 56-62.

A. Gould and J. Villumsen, *Weak lensing by nearby structures*, *Astrophys. J. Lett.* **428** (1994), L45-L48.

I. Gradshteyn and I. Ryzhik, "*Tables of Integrals, Series and Products*", Academic Press, New York, 1980.

S. Hawking and G. Ellis, "*The Large Scale Structure of Space Time*", Cambridge University Press, Cambridge, 1973.

P. Henry and J. Arnaud, *A measurement of the mass fluctuation spectrum from the cluster X-ray temperature function*, *Astrophys. J.* **372** (1991), 410-418.

S. Humit, B. Santiago, O. Lahav, M. Strauss, M. Davis, A. Dressler, and J. Huchra, *The two-point correlation function and morphological segregation in the Optical Redshift Survey*, preprint astro-ph9608001.

J. Jackson, "*Classical Electrodyamics, 2nd Ed.*", John Wiley & Sons, New York, 1975.

N. Kaiser, *Weak gravitational lensing of distant galaxies*, *Astrophys. J.* **388** (1992), 277-286.

N. Kaiser and G. Squires, *Mapping the dark matter with weak gravitational lenses*, *Astrophys. J.* **404** (1993), 441-450.

N. Kaiser, G. Squires, and T. Broadhurst, *A method for weak lensing observations*, *Astrophys. J.* **449** (1995), 460-475.

N. Kaiser, G. Squires, G. Fahlman, D. Woods, and T. Broadhurst, *Recent developments in weak lensing*, in "*Clusters of Galaxies*, ed.s F. Durret",,, 1994, pp..

M. Kamionkowski, A. Kosowsky, and A. Stebbins, *A Probe of Primordial Gravity Waves and Vorticity*, preprint astro-ph/9609132.

S. Kent, *Sloan Digital Sky Survey, Astrophys. & Space Sci.J.* **217** (1994), 27-30.

J. Loveday, S. Maddox, G. Efstathiou, and B. Peterson, *The Stromlo-APM redshift survey I: The luminosity function and space density of galaxies, Astrophys. J.* **290** (1992), 338-.

G. Luppino and N. Kaiser, *Detection of weak lensing by a cluster of galaxies at* $z = 0.83$, preprint astroph-9601194.

J. Miralda-Escudé, *The correlation function of galaxy ellipticities produced by gravitational lensing, Astrophys. J.* **380** (1991), 1-8.

J. Mould, R. Blandford, J. Villumsen, T. Brainerd, I. Smail, T. Small, and W. Kells, *A search of weak distortion of distant galaxy images by large-scale structure, M.N.R.A.S.* **271** (1994), 31-38.

J. Peebles, "*The Large Scale Structrure of the Universe*", Princeton University Press, Princeton, 1980.

I. Smail and M. Dickinson, *Lensing by distant clusters: HST observations of weak shear in the field of 3C324, Astrophys. J. Lett.* **455** (1995), L99-L102.

P. Schneider, J. Ehlers, and E. Falco, "*Gravitational Lenses*", Springer Verlag, Berlin, 1992.

C. Seitz, J. Kneib, P. Schneider, and S. Seitz, *The mass distribution of cl0939+4713 obtained from a "weak" lensing analysis of a WFPC2 image.*, astro-ph9601078.

I. Smail, R. Ellis, and M. Fitchett, *Gravitational lensing of distant field galaxies by rich clusters -I. Faint galaxy redshift distribution, M.N.R.A.S* **270** (1994), 245-270.

G. Smoot *et al.*, *Structure in the COBE differential microwave radiometer first year maps, Astrophys. J.* **396** (1992), 1-.

G. Squires, N. Kaiser, A. Babul, G. Fahlman, D. Woods, D. Neumann, and H. Böhringer, *The dark matter, gas, and galaxy distributions in Abell 2218: A weak gravitational lensing and X-ray analysis, Astrophys. J.* **461** (1996a), 572-586.

G. Squires, N. Kaiser, G. Fahlman, A. Babul, and D. Woods, *A weak gravitational lensing analysis of Abell 2390*, astro-ph9602105.

A. Stebbins, T. Mckay, and J. Frieman, *Weak lensing and the sloan digital sky survey*, in "*Astrophysical Applications of Gravitational Lensing*, ed.s C. Kochanek and J. Hewitt", Kluwer Academic Press, Dordrecht, 1996, pp. 75-80.

K. Thorne, *Multipole expansions of gravitational radiation, Rev. Mod. Phys.* **52** (1980), 299-339.

J. Tyson and P. Fisher, *Measurements of the mass profile of Abell 1689, Astrophys. J. Lett.* **446** (1995),.

J. Tyson, F. Valdes, and R. Wenk, *Detection of systematic gravitational lens galaxy image alignments: Mapping dark matter in galaxy clusters, Astrophys. J. Lett.* **349** (1990), L1-L4.

S. White, G. Efstathiou, and C. Frenk, *The amplitude of mass fluctuations in the universe, M.N.R.A.S* **262** (1993), 1023-1028.

F. Zerilli, *Tensor harmonics in canonical form for gravitational radiation and other applications, J. Math. Phys* **11** (1970), 2203-2208.